Ocean Engineering 334 (2025) 121685

Contents lists available at ScienceDirect

Ocean Engineering

journal homepage: www.elsevier.com/locate/oceaneng

Research paper

Redefining design wave conditions in the Gulf of Mexico under a changing climate

Christian M. Appendini [a,b,*], Pablo Ruiz-Salcines [a,c], Rodrigo Duran [d,e], Reza Marsooli [f], ASM Alauddin Al Azad [f], Kerry Emanuel [g]

[a] Laboratorio de Ingeniería y Procesos Costeros, Instituto de Ingeniería, Universidad Nacional Autónoma de México, Puerto de abrigo s/n, Sisal, Yucatán, 97356, Mexico
[b] Aarhus Institute of Advanced Studies, University of Aarhus, 1630, Høegh-Guldbergs Gade, Aarhus, 8000, Denmark
[c] Centre for Climate Change, Geography Department, Universitat Rovira i Virgili, Tarragona, Spain
[d] National Energy Technology Laboratory, 1450 SW Queen Ave., Albany, OR, 97321, USA
[e] Planetary Science Institute, 1700 E Fort Lowell Rd, Tucson, AZ, 85719, USA
[f] Department of Civil, Environmental and Ocean Engineering, Stevens Institute of Technology, Hoboken, NJ, 07030, USA
[g] Lorenz Center, Massachusetts Institute of Technology, Cambridge, MA, 02139, USA

ARTICLE INFO

Keywords:
Climate change
Synthetic tropical cyclones
CMIP6
Wave modeling
Extreme climate
Offshore structures
Design parameters

ABSTRACT

Climate change is expected to increase both the frequency and intensity of major tropical cyclones, raising the risk from extreme ocean waves. Reliable estimation of these waves is essential for maritime-structure design, yet assessments that rely solely on historical records cannot capture the ongoing non-stationary changes already under way. We introduce a physics-based Gulf of Mexico–wide framework that couples ~20,000 synthetic tropical cyclone events with a third-generation spectral wave model explicitly resolving present (1980–2010) and future (2070–2100, SSP5-8.5) climates using five CMIP6 GCMs. This synthetic approach overcomes the dual limitations of short observational records and coarse GCM resolution. Results show that the 100-year significant-wave height derived from present synthetic events already exceeds API values based on historical data by ~2 m, and that this design metric is projected to increase by up to 30 % by the late century in the northern Gulf. Such changes imply that structures designed today under stationary assumptions will face a higher probability of encountering their design wave during service. These findings underscore the need for robust present-day design databases and the integration of non-stationary wave climate projections into future design frameworks to safeguard maritime assets and ensure long-term resilience.

1. Introduction

Tropical cyclone (TC)-derived wind waves determine the structural design conditions for maritime structures in TC-prone regions, such as the Gulf of Mexico (GoM), where offshore oil and gas extraction activities began in 1937 (Horowitz, 2020), with continuous extraction since 1948 (Dunn, 1994). Despite the significance of waves in designing structures, there was no guidance for designing wave parameters issued during the first few decades of oil and gas activities (Dunn, 1994; Wisch et al., 2004). The American Petroleum Institute (API) established its Offshore Committee in response to the devastating impact of Hurricanes Betsy (1965) and Hilda (1964), highlighting the need for a better understanding of extreme weather events. The API released its first standard in 1969 (Wisch et al., 2004); however, design wave recommendations did not appear until the 7th edition of RP 2A in 1976, when a 100-year return period was recommended as the design wave (Mangiavacchi et al., 2005). Since then, a series of hurricanes have struck GoM oil and gas extraction areas, generating severe damage and operational downtime (Austin et al., 2008; Cruz and Krausmann, 2008; Kaiser and Yu, 2010), leading the API to update its recommended wave design parameters. After Hurricane Ivan in 2004 and the exceptionally active 2005 hurricane season, the API released updated design recommendations by dividing the GoM into different regions and provided wave design parameters for each region (API, 2007). Recognizing the severity of hurricanes (e.g. Ivan, 2004; Katrina, 2005; Rita, 2005; Ike, 2008) and the fact that a single intense hurricane or hurricane season

* Corresponding author. Laboratorio de Ingeniería y Procesos Costeros, Instituto de Ingeniería, Universidad Nacional Autónoma de México, Puerto de abrigo s/n, Sisal, Yucatán, 97356, Mexico.
E-mail address: cappendinia@iingen.unam.mx (C.M. Appendini).

https://doi.org/10.1016/j.oceaneng.2025.121685
Received 13 April 2025; Received in revised form 19 May 2025; Accepted 26 May 2025
Available online 29 May 2025
0029-8018/

can alter the extreme wave statistics (Panchang et al., 2013), the API revised its recommendations in 2014 and 2021 (API, 2014, 2021). These updates are based on historical data (Supplementary Information Text S1) and are thus necessary as new extreme events occur. The observed shift in wave statistics when recent extreme events are included suggests that the historical record alone is insufficient to provide reliable statistics, either because of data limitations or due to climate change influencing extreme wave behavior. In either case, the need for constant updates to design recommendations based on historical events leads to uncertainties in the stability of structures.

Beyond the limitations of the short historical record for allowing a robust wave climate characterization, climate change has already begun altering the climatology of tropical cyclones, with observed increases in the proportion of major hurricanes (Categories 3 to 5; Kossin et al., 2020), a trend expected to continue for Categories 4 and 5 through the end of the century (Camargo et al., 2023; Knutson et al., 2020; Pérez-Alarcón et al., 2023). As such, synthetic TCs emerge as a key tool for generating robust statistics for the present climate and projecting wave climate conditions towards the end of the century. Synthetic TC events are generated using statistical or physics-based TC models forced with large-scale oceanic and atmospheric conditions from Global Circulation Models (GCMs). The limitations and advantages of using TCs directly from GCMs, as opposed to synthetic TCs, in characterizing future TC climates were highlighted in Emanuel (2021).

Considering the advantages of synthetic events in capturing a wide range of plausible TC scenarios, including rare but high-impact events, Appendini et al. (2017) assessed the extreme wave climate in the GoM considering global warming using synthetic TCs derived from RCP 4.5 and 8.5 scenarios and two different GCMs. This past study found that the 100-year design wave height could be up to 5 m higher under global warming conditions than at present. Despite the large uncertainty imposed by using only two GCMs in deriving synthetic events, this study showed the relevance of climate change in the design parameters, as the coastal and offshore structures designed under the current wave climate will be exposed to more intense waves under future climate conditions.

Efforts made by the scientific community under the Coordinated Ocean Wave Climate Project (COWCLIP) framework (Hemer et al., 2012) have already produced wave projection ensembles —based on wind forcing directly from GCMs— to identify changes in the wave climate by the end of the century (Morim et al., 2019). Acknowledging the uncertainty associated with GCM selection and the inter-scenario variability (Wang et al., 2015), multi-method ensemble approaches have been adopted to obtain robust global wave projections (Morim et al., 2019), and distributed wind downscaling techniques have been proposed to improve accuracy in regional projections (Alizadeh et al., 2020). Nevertheless, challenges in resolving extreme waves in TC-affected areas have been acknowledged owing to the low resolution of GCMs used to force the wave models (Lobeto et al., 2021; Morim et al., 2019), which affects storm size, intensity, structure, and translational speed (Timmermans et al., 2017), and the small number of TCs in the GCMs (Mori et al., 2010). Both issues have been reported in studies related to TC projections for future climate (Camargo, 2013; Emanuel, 2010; Hill and Lackmann, 2011; Knutson et al., 2020). Recent studies have shown improvements in the representation of TCs using storm-resolving models, particularly at an approximate resolution of 5 km (Baker et al., 2024; Judt et al., 2021). However, the Coupled Model Intercomparison Project Phase 6 (CMIP6) models continue to struggle with fully resolving tropical cyclone activity and capturing peak intensities, despite improvements in HighResMIP models (Roberts et al., 2020a; Roberts et al., 2020b).

As such, relying solely on climate models for TC wave hazard assessment is insufficient as climate models currently underestimate the number of TCs and their peak intensity. Synthetic TCs offer an alternative and complementary approach that not only overcomes the underestimation of TCs inherent in low-resolution GCM and unresolved physics but also better captures the stochastic nature of TC generation and dynamics. Furthermore, synthetic TCs enable the generation of a sufficiently large dataset to reliably calculate extreme-event probabilities, an essential capability that observational time series, constrained by their limited duration and the rarity of such events, cannot practically achieve. Several studies have suggested and utilized synthetic events for quantifying extreme waves in TC-prone areas (Lobeto et al., 2021; Marsooli et al., 2021; Morim et al., 2019, 2023). This has been performed in a limited number of studies, including dynamically downscaled synthetic events for regional studies (Meza-Padilla et al., 2015) including assessment of climate change (Appendini et al., 2017) and statistically derived synthetic events (Leijnse et al., 2022). More recently, Grossmann-Matheson et al. (2024b) used statistically derived synthetic tropical cyclones to drive a parametric wave model (Grossmann-Matheson et al., 2023) and characterize global-scale TC waves conditions and extending the analysis to mid-century climate change impacts (Grossmann-Matheson et al., 2024a).

The present study utilizes a large number of dynamically downscaled synthetic TCs generated based on different GCMs to quantify climate change impacts on TC wave hazards in the GoM. By applying a fully third-generation spectral wave model, our approach not only improves the characterization of the present wave climate but also highlights the critical need for non-stationary wave climate models in the planning and design of offshore structures. This methodology provides a statistically robust framework that bridges the gap between historical observations and the evolving extremes expected under future climate scenarios, thereby offering a more reliable basis for updating industry standards.

2. Materials and methods

To assess the extreme wave climate in the GoM, we adapted the methodology of Appendini et al. (2017), as summarized in Fig. 1. The extreme wave climate was quantified using synthetic TCs derived from reanalysis and GCMs as described in Section 2.1, from which we created wind fields using a parametric wind model to force a third-generation wave model. The following subsections summarize each methodological step.

2.1. Synthetic TC database

Synthetic TC events were generated by the statistical/deterministic TC model described in Emanuel et al. (2006, 2008) and Emanuel (2013). As summarized in Appendini et al. (2017), the generation of synthetic events consists of random seeding of warm-core vortices across the ocean with peak wind speeds of 12 m/s that can either develop (by reaching an intensity of at least 21 m/s) or decay according to large-scale oceanic and atmospheric conditions. TCs are steered using a beta-and-advection model (Marks, 1992), and the TC intensity is calculated along each track position using the deterministic, coupled ocean-atmosphere hurricane model described in Emanuel (2004). Both models use synthetic wind time series at 250 and 850 hPa, represented as a Fourier series of random phases, constrained to have monthly means, variances, and covariances calculated using daily data from reanalyses or GCM, and to have a geostrophic turbulence power-law distribution of kinetic energy Emanuel et al. (2008). Hence, the tracks and forward velocities are determined based on ambient circulation conditions. The intensity model also considers the monthly mean potential intensity and 600 hPa saturation deficit derived from the reanalysis or GCM (Emanuel, 2013). The deterministic synthetic events used in this study provide an advantage over the statistically derived events, for example, from the STORM database (Bloemendaal et al., 2022) used in Grossmann-Matheson et al. (2024a), as they are not constrained by present-day statistics. This allows our model to capture a broader spectrum of TC intensities and behaviors, including extreme scenarios that may not be reflected in historical records.

The synthetic TCs databases for present and future climates encompass events generated based on five different GCMs from the CMIP6:

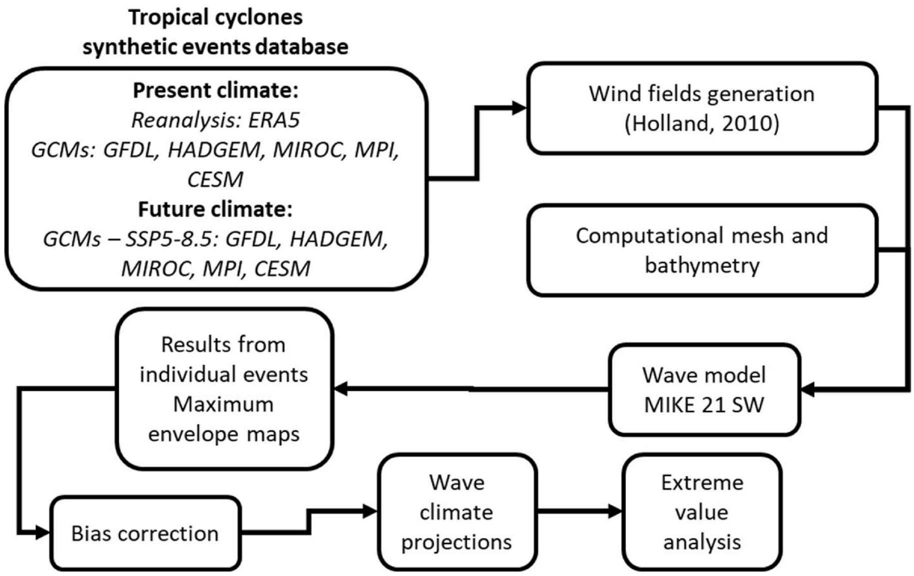

Fig. 1. Flow diagram of the method employed in this study.

GFDL, HADGEM, MIROC, MPI, and CESM (refer to Table 1 for the complete name of each model, version, and reference). The five GCMs were selected to balance model diversity (in terms of geographic origin) and data availability (complete atmospheric/oceanic fields at the required temporal resolution for TC generation), ensuring coverage of the dominant sources of inter-model variability while maintaining a computationally feasible ensemble. The present climate is considered from 1980 to 2010 and the future climate from 2070 to 2100. For the future climate, we used the Shared Socio-economic Pathway 5 scenario with a radiative forcing of 8.5 W per square meter (SSP5-8.5). The synthetic events were generated for the entire North-Atlantic basin and each database consisted of 10075 events for the GCM-derived and 20500 reanalysis-derived events. Given the focus of this study on the GoM and considering that TC-derived waves are centered near the TC track (Shi et al., 2024), we followed Appendini et al. (2017) and only used synthetic TCs entering the GoM and western Caribbean Sea. The number of TCs entering the GoM was a subset of each database, as shown in Table 2, and was used to force the wave model.

Table 1
Global Circulation Models used to derive present and future climate synthetic tropical cyclones.

Institution	Model name and version	Name used in this article	Reference
National Oceanic and Atmospheric Administration/ Geophysical Fluid Dynamics Laboratory (NOAA/GFDL)	Earth System Model 4 (GFDL-ESM4)	GFDL	Dunne et al. (2020)
UK Met Office	Hadley Global Environmental Model 3 (HadGEM3-GC31-LL)	HADGEM	Sellar et al. (2020)
Center for Climate System Research/ National Institute for Environmental Studies/Japan Agency for Marine-Earth Science and Technology	Model for Interdisciplinary Research on Climate 6 (MIROC6)	MIROC	(Tatebe et al., 2019)
Max Planck Institute	Earth System Model MPI-ESM1-2-HR	MPI	Müller et al. (2018)
National Center for Atmospheric Research	Community Earth System Model 2	CESM	Danabasoglu et al. (2020)

2.2. Wind field definition

The synthetic datasets provide storm parameters for each TC, including the date, time, position of the TC center (eye), radius of maximum winds, and maximum wind speeds. These parameters can be used to generate the TCs wind fields using a parametric wind model. We use the Holland model (Holland et al., 2010), a standard parametric wind model (Eq. (1)) commonly used in hurricane storm surge and wave hazard assessments (Leijnse et al., 2022; Martínez-Asensio et al., 2013), to generate wind fields based on the given TC parameters.

$$V_r = V_m\left(\left(\frac{R_{mw}}{r}\right)^{b_s} e^{\left(1-\left(\frac{R_{mw}}{r}\right)^{bs}\right)}\right)^x \quad \text{Eq. (1)}$$

where R_{mw} is the radius of maximum winds, V_m is the maximum wind speed, r is the radial distance from the eye of the hurricane to any given point surrounding it, and V_r is the wind speed of the hurricane at radius r. Parameter b_s is related to the original B Holland parameter ($b_s = B\, g_s^x$) being g_s a reduction wind gradient to surface factor, and x is the scaling parameter that adjusts the profile shape. We applied a constant b_s value of 1.8 and the parameter x varied linearly with the radius, as described in Eq. (2).

$$x = \begin{cases} 0.5 & r \le R_{mw} \\ 0.5 + (r - R_{mw})\dfrac{x_n - 0.5}{r_n - R_{mw}} & r > R_{mw} \end{cases} \quad \text{Eq. (2)}$$

Table 2
Number of synthetic TC events used to characterize the present and future wave climate in the Gulf of Mexico.

Model	Present climate (1980–2010)	Future climate (2070–2100)
ERA5	5082	NA
GFDL	4354	4032
HADGEM	3557	2015
MIROC	4640	4149
MPI	6279	6019
CESM	4306	3360

where x_n is the adjusted exponent to fit the peripheral observations at radius r_n.

The effect of the surface background winds was included by adding storm translation velocity, which is calculated using the time and position (trajectory) of synthetic storms.

The synthetic 10-m wind data is a 1-min average sustained wind. Nevertheless, the ocean surface responds to wind stress over longer timescales (Powell et al., 1996). We applied a gust factor G_f to convert the 1-min average to the 10-min average sustained wind as follows (Powell et al., 2010; Powell and Houston, 1996):

$$V_{Avg}^{T} = \frac{V_{1\ min}^{T}}{G_f} \quad \text{Eq. (3)}$$

where $V_{1\ min}^{T}$ is the 1-min average sustained wind, V_{Avg}^{T} is the resultant wind "T"-min average wind, and G_f is the gust factor. We used a factor of 1.11 to convert 1-min to 10-min sustained wind following Powell et al. (2010) and Powell and Houston (1996). The resulting wind fields have a resolution of 0.05°.

2.3. Wave modeling

The generated wind fields for each TC were used to force the MIKE 21 SW spectral wave model (Sørensen et al., 2004). This model is a flexible mesh finite volume model based on the wave action equation, and is used to simulate the growth, decay, and transformation of wind-generated waves and swells in coastal and offshore regions. The model is formulated in terms of the mean wave direction, θ, and the relative angular frequency, σ, where the action density, $N(\sigma, \theta)$, is related to the energy density, $E(\sigma, \theta)$, using Eq. (4).

$$N(\sigma, \theta) = \frac{E(\sigma, \theta)}{\sigma} \quad \text{Eq. (4)}$$

We employed the wave action balance equation formulated in spherical coordinates, where the evolution of the wave spectrum in the position given by latitude ($\varnothing$), and longitude (λ) at a particular time (t), as given by Eq. (5).

$$\frac{\delta N}{\delta t} + \frac{\delta}{\delta \varnothing} c_{\varnothing} N + \frac{\delta}{\delta \lambda} c_{\lambda} N + \frac{\delta}{\delta \sigma} c_{\sigma} N + \frac{\delta}{\delta \theta} c_{\theta} N = \frac{S}{\sigma} \quad \text{Eq. (5)}$$

in Eq. (5), C represents the phase velocity, whereas the energy source term S is composed of multiple energy source/sink functions. These functions describe the various physical processes that occur during the generation, decay, and transformation of waves, as shown in Eq. (6).

$$S = S_{in} + S_{nl} + S_{ds} + S_{bot} + S_{surf} \quad \text{Eq. (6)}$$

where S_{in} represents the wind energy input given by a linear and a nonlinear growth rate (Janssen, 1989, 1991; Janssen et al., 1989); S_{nl} interactions (Hasselmann et al., 1985; Hasselmann and Hasselmann, 1985; Komen et al., 1994) and triad-wave interactions (Eldeberky and Battjes, 1995, 1996); S_{ds} is the energy dissipation due to whitecapping; (Komen et al., 1994) S_{bot} is the energy dissipation due to bottom friction (Johnson and Kofoed-Hansen, 2000); and S_{surf} is the energy dissipation due to depth-induced wave breaking (Battjes and Janssen, 1978; Eldeberky and Battjes, 1996). The spatial discretization of the equations is based on a centered finite volume method over unstructured meshes. More details on the source terms, discretization of the governing equation, time integration, and model parameters are provided in Sørensen et al. (2004).

The wave model domain encompassed the GoM and the western Caribbean Sea, with closed and fully absorbing boundaries at 80°W longitude and 15°N latitude, so that no external wave action entered the model domain. This choice assumes that the swell generated in the North-Atlantic and central/eastern Caribbean Sea has negligible influence in the GoM (Appendini et al., 2014), with the goal of capturing only the wave field generated by each TC simulated. For each synthetic storm the simulation commenced 24 h before the cyclone center crossed the domain boundary and ended 12 h after it exited, thereby capturing the leading and trailing wind fields that govern wave growth within the mesh. The computational mesh was based on triangular elements of approximately 10 km in the offshore area, with increasing resolution towards the coast. The bathymetry data were obtained from the Coastal Relief Model (NOAA National Centers for Environmental Information, 2023), available local surveys for Mexican coastal areas, and ETOPO1 bathymetric data (Amante and Eakins, 2009) for areas not covered by the first two databases (Fig. 2).

The numerical setup considered the fully spectral and non-stationary time formulation, with a directional discretization for 360° divided into 32 directions and a logarithmic spectral discretization with a minimum frequency of 0.05 Hz, 25 frequencies, and a frequency factor of 1.1. The increased directional discretization in comparison to Appendini et al. (2017) was to mitigate the garden sprinkler effect (Tolman, 2002). The time step followed a multisequence integration method, with a minimum step of 0.01 s and a maximum of 3600 s. Quadruplet wave interactions are included for energy transfer. A wave-breaking factor with a constant gamma value of 0.80 and an alpha value of 1.0 was used. The bottom friction was represented by a constant Nikuradse roughness value of 0.002 m. We employed whitecapping dissipation coefficients *Cdis* and *Deltadis* set to values of 3.5 and 0.6, respectively, where *Cdis* primarily influences the wave height and *Deltadis* affects the wave period. A JONSWAP fetch growth expression with shape parameters a and b of 0.07 and 0.09 respectively, was used as the initial condition, and the peakness parameter was 3.3. The offshore boundaries at the Caribbean Sea and Florida Strait were considered closed, where no waves entered the model domain, and the outgoing waves were fully absorbed, as in Appendini et al. (2017).

2.4. Wave model validation

Wave model evaluation was conducted by simulating historical TC events from 1975 to 2020 and comparing the model results to National Data Buoy Center (NDBC) buoys and satellite altimetry measurements of wave height using the database from Tamizi and Young (2024). The compiled altimetry dataset combines information from various sources, including in situ buoy measurements and satellite-based remote sensing data. It encompasses observations from altimeters, scatterometers, and radiometers for 2927 global TCs. These historical events were derived from The International Best Track Archive for Climate Stewardship (IBTrACS) dataset (Knapp et al., 2010), covering 1985 to 2017. As described by Tamizi and Young (2024), wave height data from satellite altimeters, obtained from the Australian Ocean Data Network archive, have undergone calibration using buoy measurements.

For evaluation with the altimeter database, we used all historical events with altimeter observations in the GoM between 1985 and 2017, for a total of 273 observations. We compared the model results for each event with observations that fell within three times the radius of maximum winds from the TC eye position, as obtained from the IBTrACS dataset. We selected Hs from the model at the same position for each satellite-observed Hs value. The original track observations are provided in the database at their original resolution (6 h in most cases), assigning observations at each track position within the 3 h prior and subsequent. The historical events were modeled with a temporal resolution of 1 h; thus, satellite observations were aligned with the next hour of simulated data (30 min after and before).

Fig. 3a illustrates the modeled wave field for Hurricane Claudette in 2003 on July 13th at 04:00 h alongside ENVISAT satellite observations, whereas Fig. 3b presents the time series of observed and simulated data within three times the radius of maximum winds at this time frame. The inverse cumulative distributions or quantile function comparing the model results and all the satellite observations and the error indexes are shown in Fig. 3c, showing a good agreement between simulated and

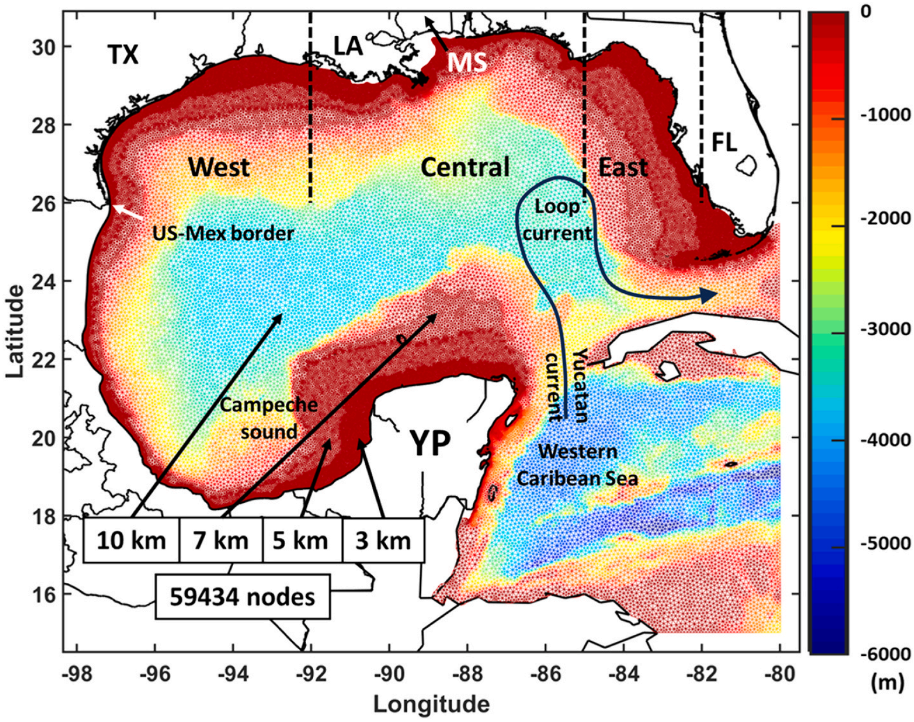

Fig. 2. Wave model's computational mesh and bathymetry, denoting the areas referred to in the article. The vertical dash lines delineate the API (2021) areas in the US with a south limit at latitude 26°N. Acronyms for text in figure: TX, Texas; LA, Louisiana; MS, Mississippi; FL, Florida; YP, Yucatan Peninsula; Mex, Mexico.

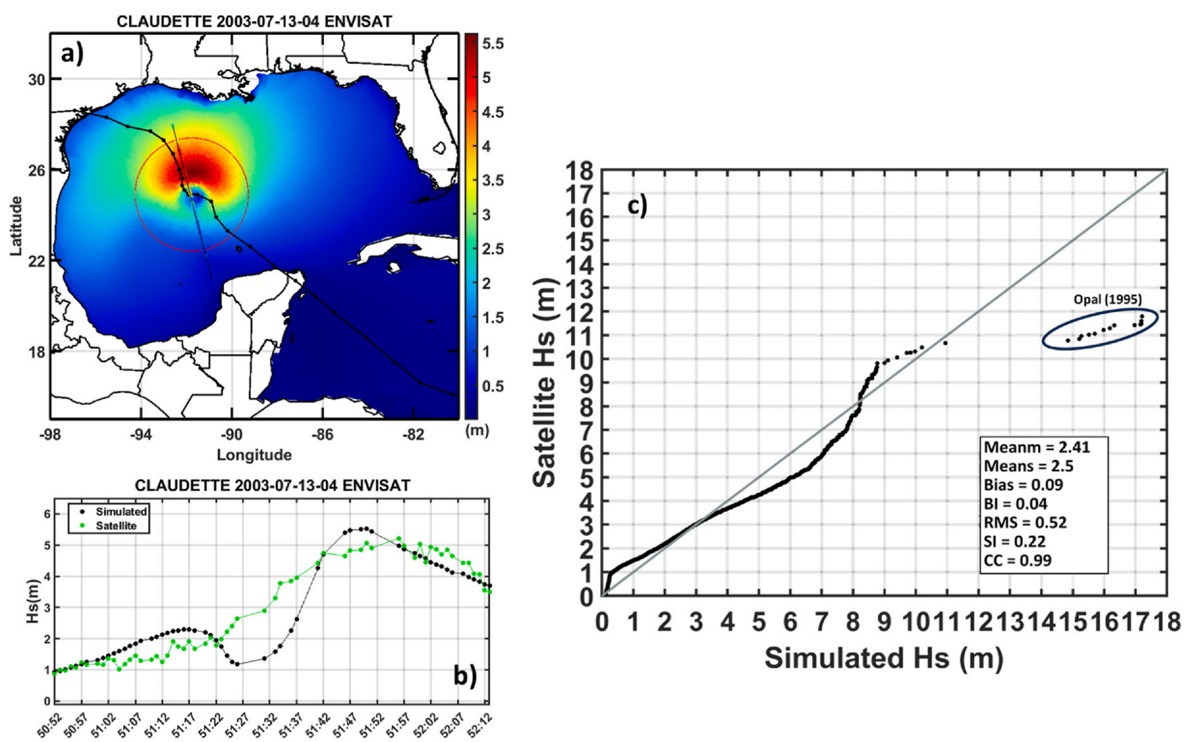

Fig. 3. a) Modeled wave field map for Hurricane Claudette 2003 on July 13th at 04:00 h and ENVISAT satellite observations. The black line corresponds to the storm track, and the red circle denotes the circular area within 3 times the radius of maximum winds. b) Time series of observed and simulated significant wave height (Hs) data within the area within 3 times the radius of maximum winds at this moment. c) QQ plot for observed Hs values from all historical simulated events and altimeter data within the area within 3 times the radius of maximum winds. (For interpretation of the references to color in this figure legend, the reader is referred to the Web version of this article.)

measured data, except for the overestimation of waves from Hurricane Opal (1995), which was close to the shore during the ERS 1 satellite measurements.

The model evaluation was also performed using in-situ measurements from NDBC buoys 42001, 42002, 42003, 42039, 42040, and 42055 located in the deep waters of the GoM and buoy 42056 located in the western Caribbean Sea. Buoy data were included in the evaluation when two criteria were satisfied: 1) the TC event was located within an area three times the radius of maximum winds from the buoy to the TC eye position, and 2) the event reached at least tropical storm intensity at some point within the area. We used the storm parameters from the Tropical Cyclone Extended Best Track Dataset (Demuth et al., 2006) to select storms that met the latter criterion. Comparisons were performed for simulated events between 1975 and 2020. Table 3 shows the error indices obtained by comparing the model results to measurements through their inverse cumulative distributions or quantile functions for each event. The error statistics were calculated for each event using the equations described in the Supplementary Information (Text S2). The average error for all events is presented in Table 3 for each buoy, while Fig. 4 shows the quantile function plot, considering only the maximum Hs value for the observed data from the NDBC and simulated events.

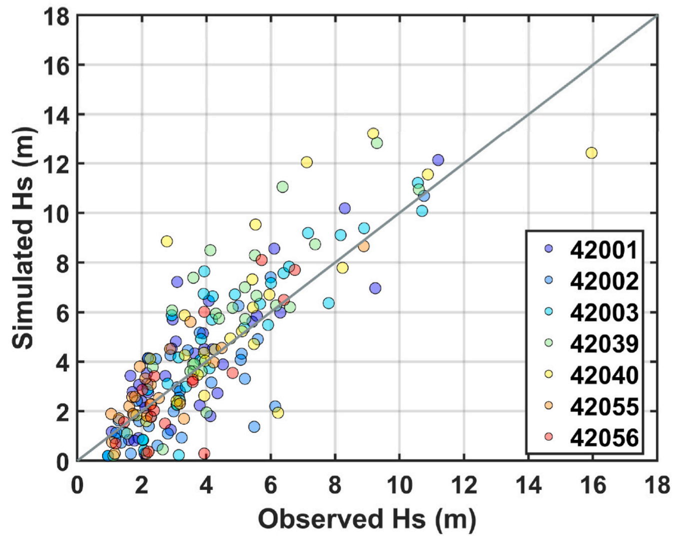

Fig. 4. QQ plot comparing observations from NDBC and model results for maximum significant wave height (Hs). Each data point represents the maximum HS during a historical TC event.

2.5. Wave climate analysis

We generated a maximum envelope map of Hs for each synthetic event by selecting the highest Hs value at each grid point during the event passage. Thus, the number of maps equals the number of synthetic events (Table 2). Using the Hs maximum envelope maps, we applied a Bias Correction method at each grid point (see Section 2.6, Bias Correction) and characterized the extreme wave climate based on the mean values and specific percentiles.

We assessed the extreme wave probability via return periods at each of the 59,434 grid nodes by assembling bias-corrected maximum Hs vectors for all synthetic events in both present and future climates. We then applied a peak-over-threshold (POT) approach by using a fixed 98th-percentile threshold and fit a Generalized Pareto Distribution (GPD; Coles, 2001) to these exceedances, yielding Hs for specified return periods and mapping the results. Because threshold and distribution choice strongly influence POT outcomes (Méndez et al., 2006), we tested automated threshold selection (Caires, 2016) and alternative distributions (e.g. Baghanian and Alizadeh, 2022). While the automated method often performed well, it sometimes selected thresholds yielding high shape parameter values, resulting in divergent asymptotic behavior and unrealistically large wave heights for long return periods. By contrast, the fixed 98th-percentile threshold with GPD produced stable, physically plausible estimates. Considering that GPD is the suggested distribution when using the POT method (Coles, 2001) and it is widely adopted for TC hazard assessment (Jamous et al., 2023; Marsooli et al., 2021), we applied this procedure across all nodes and models. We then generated maps for the selected return periods using the corresponding values at each grid element.

To compare our wave hazards with those from the API latest guidelines (API, 2021), we also calculated return periods for each of the API regions in the GoM. To determine the return periods in the API areas, we select the grid points corresponding to each area.

- Western GoM between 92° W and 98° W.
- Central GoM between 85° W and 92° W.
- Eastern GoM between 82° and 85° W.

We merged the data corresponding to each API area and performed the same extreme value analysis described above, using the 98th-percentile as the threshold for POT. The procedure described above is a simplified version of the grid pooling methods from Heideman and Mitchell (2009), which presented a procedure for grid pooling at a specific point location. Grid pooling is performed in API recommendations so that the randomness of the TC tracks is diffused by assessing the wave conditions as similar in a particular area. Nevertheless, the grid pooling procedure for each area is not described in API (2014, 2021). Return period waves were calculated for each GCM-derived wave dataset. Using these values, we calculated the ensemble mean and uncertainty envelopes based on a single standard deviation.

2.6. Bias correction

Recognizing that biases inherent in GCMs can propagate into the derived wind fields and, consequently, to wave simulations (Wang et al., 2015), a more robust assessment can be achieved using multi-model ensembles (Morim et al., 2019). Alternatively, downscaling techniques that incorporate bias-corrected winds can improve the accuracy of wave projections (Alizadeh et al., 2020). In our case, GCM biases propagate through our synthetic-TC generation process; therefore, we applied bias

Table 3
Statistics from model evaluation using historical events from 1975 through 2020. $Mean_m$ and $Mean_s$ are, respectively, the mean values from the buoy (measured) data and simulated data; BI is bias index, RMS is root mean squared error, SI is scatter index, and CC is correlation coefficient.

Parameter	Buoy	Num. events	$Mean_m$	$Mean_s$	Bias	BI	RMS	SI	CC
Hs (m)	**42001**	37	2.80	2.87	0.07	0.03	0.99	0.41	0.94
	42002	32	2.57	1.87	−0.69	−0.27	1.12	0.47	0.93
	42003	32	3.44	3.50	0.06	−0.03	1.22	0.45	0.94
	42039	28	3.43	3.74	0.31	0.04	1.33	0.43	0.94
	42040	26	4.03	4.10	0.07	0.05	1.48	0.39	0.94
	42055	21	2.02	1.75	−0.27	−0.13	0.87	0.52	0.92
	42056	17	2.48	2.08	−0.40	−0.17	1.15	0.47	0.92
	all	193	2.97	2.84	−0.12	−0.07	1.17	0.45	0.93

correction directly to the resulting wave outputs rather than to the raw GCM winds themselves. Our bias correction aims to improve the statistical consistency of simulated wave climate based on GCM data with observational or reference model data by defining a transfer function that adjusts GCM outputs, allowing for the correction of future projections from the same GCM. We implemented a hybrid bias-correction method designed specifically for synthetic TCs to correct biases in wave conditions derived from GCM-based synthetic events when compared to the wave climate from a reference model, which is the ERA5-based synthetic events in our study. The proposed methodology combines two approaches: the empirical quantile mapping technique (EQM; Déqué, 2007) and an enhancement of extreme value representation using a Gumbel extreme value distribution fit.

The EQM adjusts the empirical cumulative distribution function (CDF) of the GCM-derived TC wave height for the present period to match the CDF of the same variable from the reference model (i.e. ERA5-derived TC waves) for the same period. The CDFs of the GCM and the reference model are mapped using a discrete number of quantiles, and linear interpolation is applied to define a transfer function (Eq. (7)).

$$H_{cor} = \mathrm{CDF}_{Ref}^{-1}\left[CDF_{GCM}(H)\right] \quad \text{Eq. (7)}$$

where $\mathrm{CDF}_{\mathrm{Ref}}$ is the cumulative distribution function of the reference dataset, $\mathrm{CDF}_{\mathrm{GCM}}$ is the cumulative distribution function of a GCM, H is the original GCM value, and $\mathrm{H}_{\mathrm{cor}}$ is the corrected value. Assuming that the bias in the GCM-based present wave conditions remains the same for future projections, the transfer function is then applied to each GCM dataset for the future climate period. This allows us to calculate bias-corrected wave projections for future periods.

A known limitation of the EQM method is its handling of extreme values, especially when there is a need to extrapolate data (Li et al., 2010; Rohith and Cibin, 2024). When the GCM-based wave data for present or future climates exceed the maximum observed values in the reference dataset, values will fall beyond the transfer function and, thus, an extrapolation will be required. Déqué (2007) proposed a simple extrapolation based on a constant correction factor using the last available quantile in the present climate GCM-based data. However, for TCs, where future intense events may not be well represented in the present climate record, this approach could introduce biases into future climate projections.

To better capture extreme events, we complemented the EQM method with a parametric quantile mapping technique that adjusts the distribution applied to extreme values before computing the CDF. The key distinction between this method and the EQM method lies in the calculation of the CDF. Here, we propose the use of the Gumbel distribution, which is a special case of the extreme value family with a shape parameter $\xi = 0$. The CDF is given by Eq. (8).

$$CDF\,(H;\ \mu;\ \sigma) = \exp\left(-\exp\left(-\frac{H-\mu}{\sigma}\right)\right) \quad \text{Eq. (8)}$$

where μ and σ are location and scale parameters, respectively. The bias correction was initially applied using the classic quantile mapping method, followed by the Gumbel distribution fit to extend the upper tail. This approach avoids direct extrapolation and improves the extreme value representation.

In addition to the Gumbel distribution, other distributions were tested for bias correction of our generated GCM-based wave data using parametric methods (Parker and Hill, 2017). The Gumbel function was chosen because, in the case of TC, we often encountered extrapolation challenges when one of the fitted distributions has either a bounded upper tail or a heavy tail. Additionally, Lobeto et al. (2021) applied the Gumbel function successfully for bias correction in wave modeling.

The number of quantiles used in the bias correction process significantly influenced the performance of the method. Given that this study focused on the maximum wave heights generated by each TC event, we opted to select a high number of quantiles to achieve the best possible fit.

To sum, our method for bias correction is applied to each computational grid node following the following steps.

1. Quantile definition: Quantiles cover the range from 0.01 (q01) to 0.999 (q999), with linearly distributed quantiles from 0.05 (q05) to 0.999 (q999) with an increment of 0.001.
2. EQM application: The EQM method is applied to all generated wave data, generating bias-corrected wave characteristics for each GCM-based dataset in both present and future climates (including extreme values).
3. Extreme Value Adjustment: If extrapolation is required (e.g., when future values exceed present wave climate values or present values surpass the ERA5 reference dataset), extreme values are adjusted using the parametric quantile mapping technique. The Gumbel distribution is fitted to values above the 98th-percentile threshold, and bias-corrected extreme values for both the present and future CDFs of wave characteristics are obtained, similar to the EQM method.
4. Replacement of Extreme Values: Only extreme values that required extrapolation in the EQM process are substituted with Gumbel-adjusted corrections obtained from step 3.

Because synthetic TCs generated using GCMs and ERA5 reanalysis show differences in the annual frequency of occurrence, the method requires adjusting the event frequency to match historical records. The ERA5 and each GCM dataset frequency were bias-corrected relative to the historical frequency for the period 1980–2010. The future climate annual frequency was obtained by multiplying the GCM-derived synthetic frequency in future climate by the percentage change in each GCM-derived frequency in the present climate with respect to the historical record frequency.

3. Results and discussion

3.1. Bias assessment and correction for waves derived from GCM synthetic events

The wave model was forced with synthetic TC datasets generated based on ERA5 reanalysis and GCMs to characterize the wave climate from each dataset. As described previously, the ERA5-derived wave climate was used as a baseline to assess the bias of the present wave climate from GCM-derived synthetic events. Using the resulting maximum significant wave heights (Hs) for each synthetic dataset, we computed the mean, 90th-, 95th-, and 99th-percentiles (Fig. 5) and calculated the bias for each of the GCMs (Fig. 6).

For a clearer discussion, we divide the model domain into the following sectors: the northwestern (NW), northeastern (NE), southwestern (SW), and southeastern (SE) sectors. The NW events affect the offshore areas of Texas, Louisiana, and northern Mexico; the NE events affect offshore areas of West Florida and Mississippi, as well as the northern part of the loop current area; the SW events affect the Campeche sound; the SE events affect the western Caribbean Sea, the Yucatan current, and the southern part of the loop current.

The results under the present climate (1980–2010) showed similar wave patterns for all GCMs (Fig. 5), where the largest wave heights were found in the northern section of the GoM (NW and NE) and the western Caribbean Sea (SE), whereas the Campeche sound region (SW) showed smaller TC-derived waves. Synthetic wave data based on HADGEM and MIROC showed milder events than the other GCMs, and particularly for HADGEM, the wave heights were particularly small in the SE.

The bias in mean Hs (Fig. 6a–e,i,m,q), calculated relative to ERA5-derived TC waves, shows high variability between models, with the most overestimation in the NW (GFDL, CESM, and MPI) and NE (HADGEM, GFDL, CESM, and MIROC) sectors. All GCMs underestimate Hs in the SW sector, and the largest underestimation is calculated in the SE sector based on HADGEM, CESM, and MIROC. Similar bias patterns were obtained for the different percentiles of Hs, although the bias for

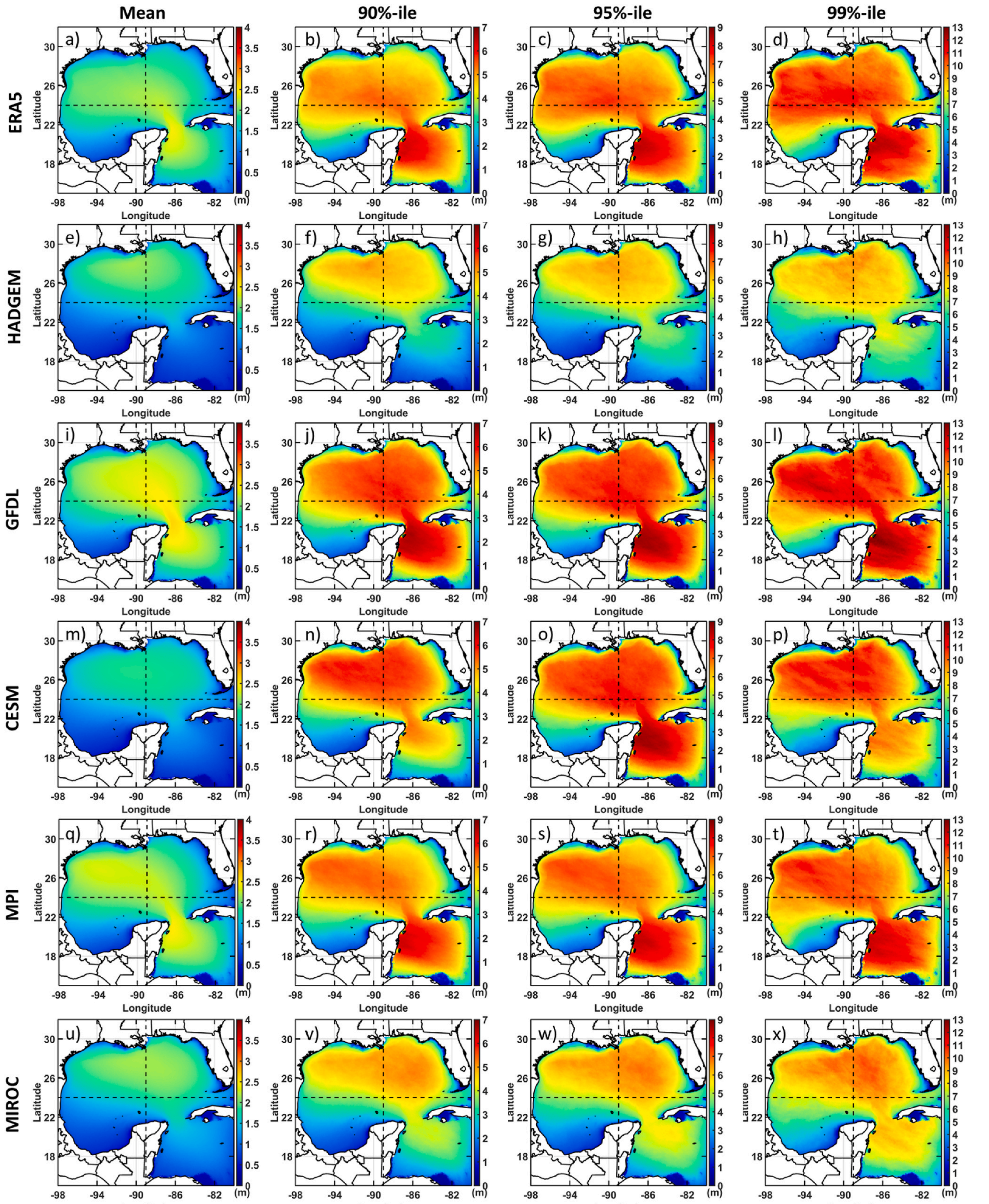

Fig. 5. Statistics of significant wave heights calculated for the synthetic TCs from GCMs and ERA5 datasets for the present climate (1980–2010). GCMs-based data are original (pre-bias-corrected) data. Panels represent ERA5 (a, b, c, d), HADGEM (e, f, g, h), GFDL (i, j, k, l), CESM (m, n, o, p) MPI (q, r, s, t) and MIROC (u, v, w, x) including mean (a, e, i, m, q, u), 90 %-ile (b, f, j, n, r, v), 95 %-ile (c, g, k, o, s, w) and 99 %-ile (d, h, l, p, t, x).

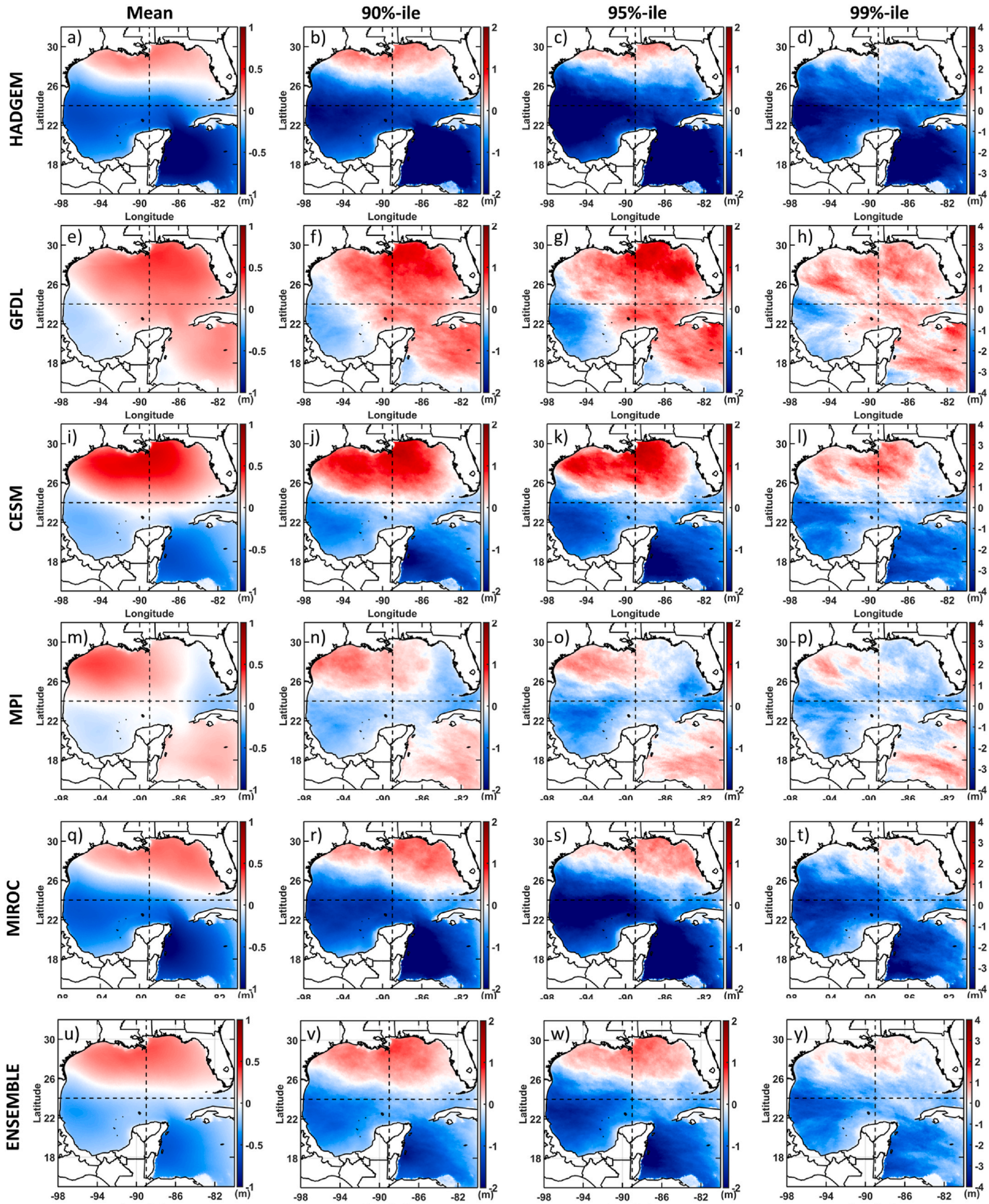

Fig. 6. Bias in significant wave height calculated based on GCM-based synthetic TCs compared to the ERA5 synthetic TCs. GCM-based datasets are HADGEM (a, b, c, d), GFDL (e, f, g, h), CESM (i, j, k, l), MPI (m, n, o, p), MIROC (q, r, s, t) and Ensemble (u, v, w, x) considering mean (a, e, i, m, q, u), 90 %-ile (b, f, j, n, r, v), 95 %-ile (c, g, k, o, s, w) and 99 %-ile (d, h, l, p, t, x).

the 99th-percentile (Fig. 6d–h,l,p,t) was less spatially smooth. GFDL and CESM show stronger overestimation in the northern GoM than the other GCMs across all percentiles, whereas HADGEM and MIROC show higher underestimations for the southern GoM and the western Caribbean Sea. In particular, HADGEM shows a large underestimation, except near the US coastal areas, where there is a slight underestimation, except for the 99th-percentile. For the ensemble (Fig. 6u,v,w,x), there was a clear separation of the bias, with the northern area being overestimated and the southern area underestimated.

The calculated biases are removed from the GCM-based wave heights. After bias correction, the resulting present wave climate is shown in Fig. 7, which shows similar patterns in the wave height across different models, validating the bias correction method.

3.2. Future wave climate assessment

Fig. 8 shows the future wave climate (2070–2100) obtained for each of the bias-corrected GCM-based synthetic events, while Fig. 9 shows the

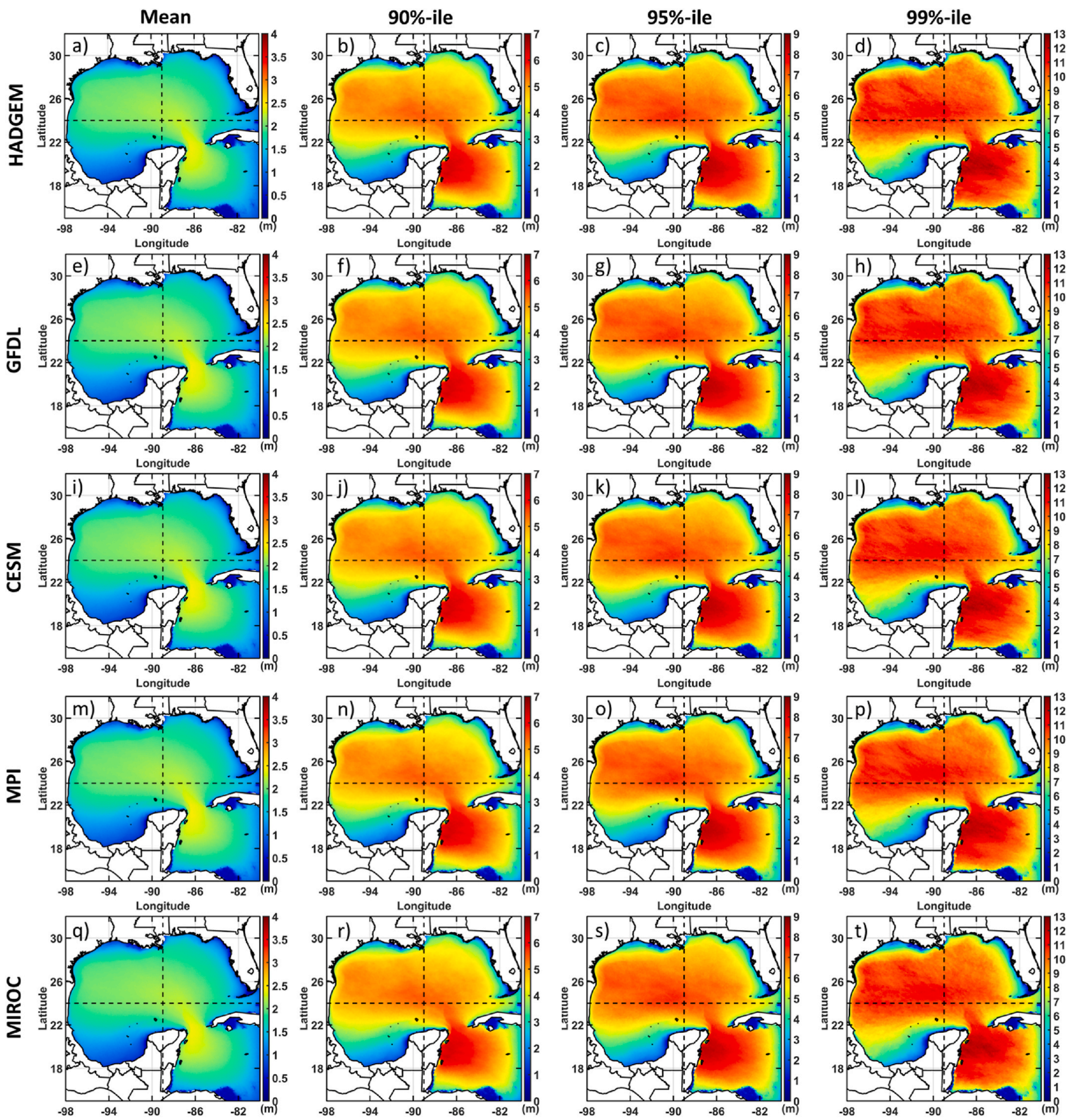

Fig. 7. Bias corrected significant wave height for GCM-based datasets in the present climate (1980–2010) for HADGEM (a, b, c, d), GFDL (e, f, g, h), CESM (i, j, k, l), MPI (m, n, o, p) and MIROC (q, r, s, t) including mean (a, e, i, m, q), 90 %-ile (b, f, j, n, r), 95 %-ile (c, g, k, o, s) and 99 %-ile (d, h, l, p, t).

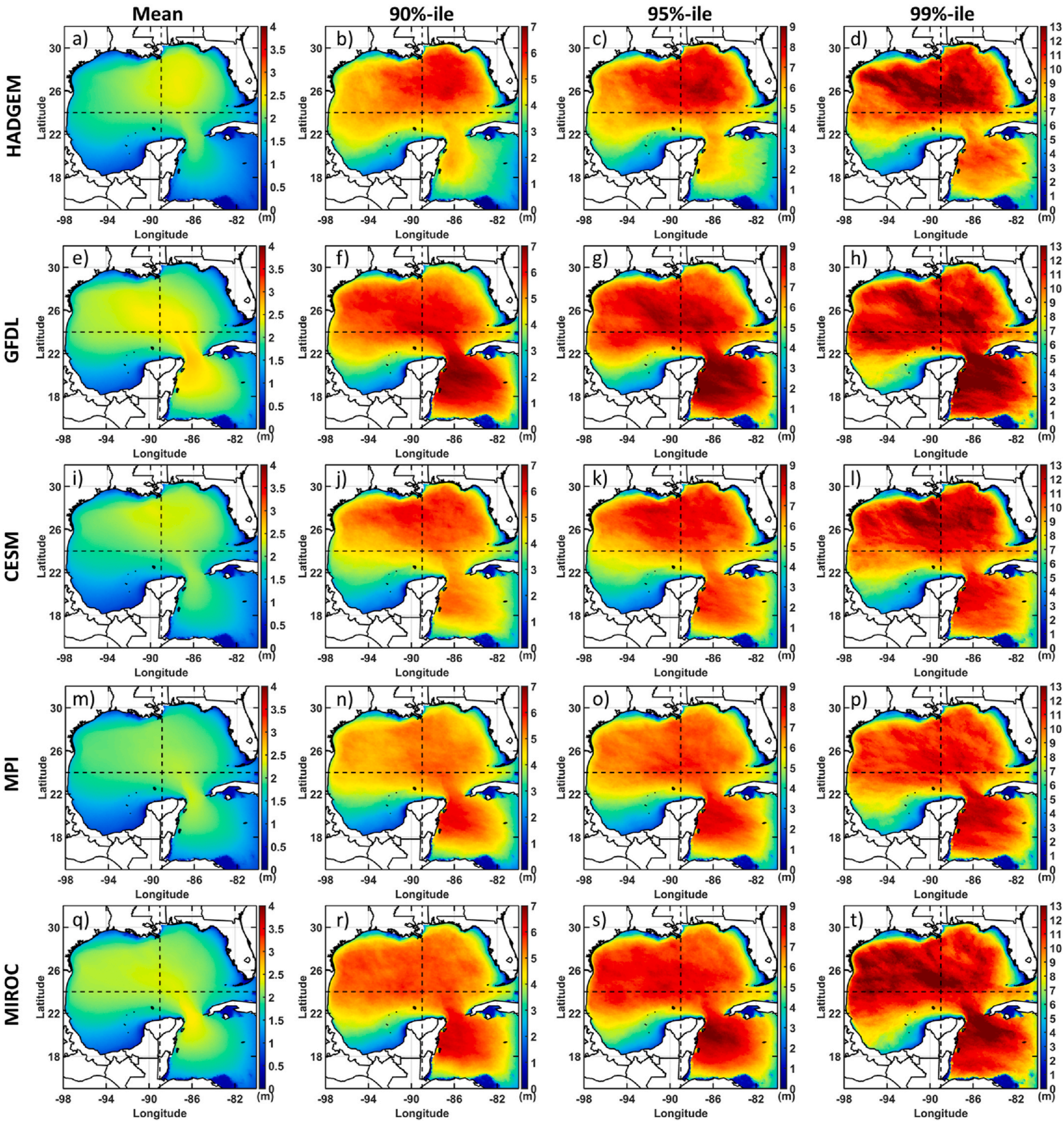

Fig. 8. Bias corrected significant wave height in a future climate (2070–2100) for GCM datasets HADGEM (a, b, c, d), GFDL (e, f, g, h), CESM (i, j, k, l), MPI (m, n, o, p) and MIROC (q, r, s, t) including mean (a, e, i, m, q), 90 %-ile (b, f, j, n, r), 95 %-ile (c, g, k, o, s) and 99 %-ile (d, h, l, p, t).

bias-corrected GCM model ensemble results for the present and future climate, as well as the magnitude and percentage of the change in Hs. In the future climate, we found that the wave patterns are similar across GCMs, with the largest waves in the NW, NE, and SE sectors. The largest waves in the NE and NW sectors were found for the HADGEM, GFDL, CESM, and MIROC. GFDL and MIROC show more intense events in the SE, except for the highest waves (i.e. 99th-percentile) where they are of similar intensity to the events in the northern GoM. HADGEM showed the mildest events in the SE, whereas MPI showed milder events in general. For the SW sector, the patterns are similar across the GCM datasets, except for the northern part of the sector, which follows the results for the NW sector.

The model ensemble results in Fig. 9 reveal consistent spatial patterns in Hs distribution across the GoM. However, analyses of both the absolute changes (Fig. 9i–l) and percentage changes (Fig. 9m–p) indicate that the change in Hs is not uniform across all sectors or percentiles. Notably, the SE sector shows a decrease in Hs for the mean and 90th- and 95th-percentiles, with milder increases for the 99th-percentile compared to the NW sector, which could reflect the probable shift of TC towards the poles (Kossin et al., 2014; Studholme et al., 2022). The

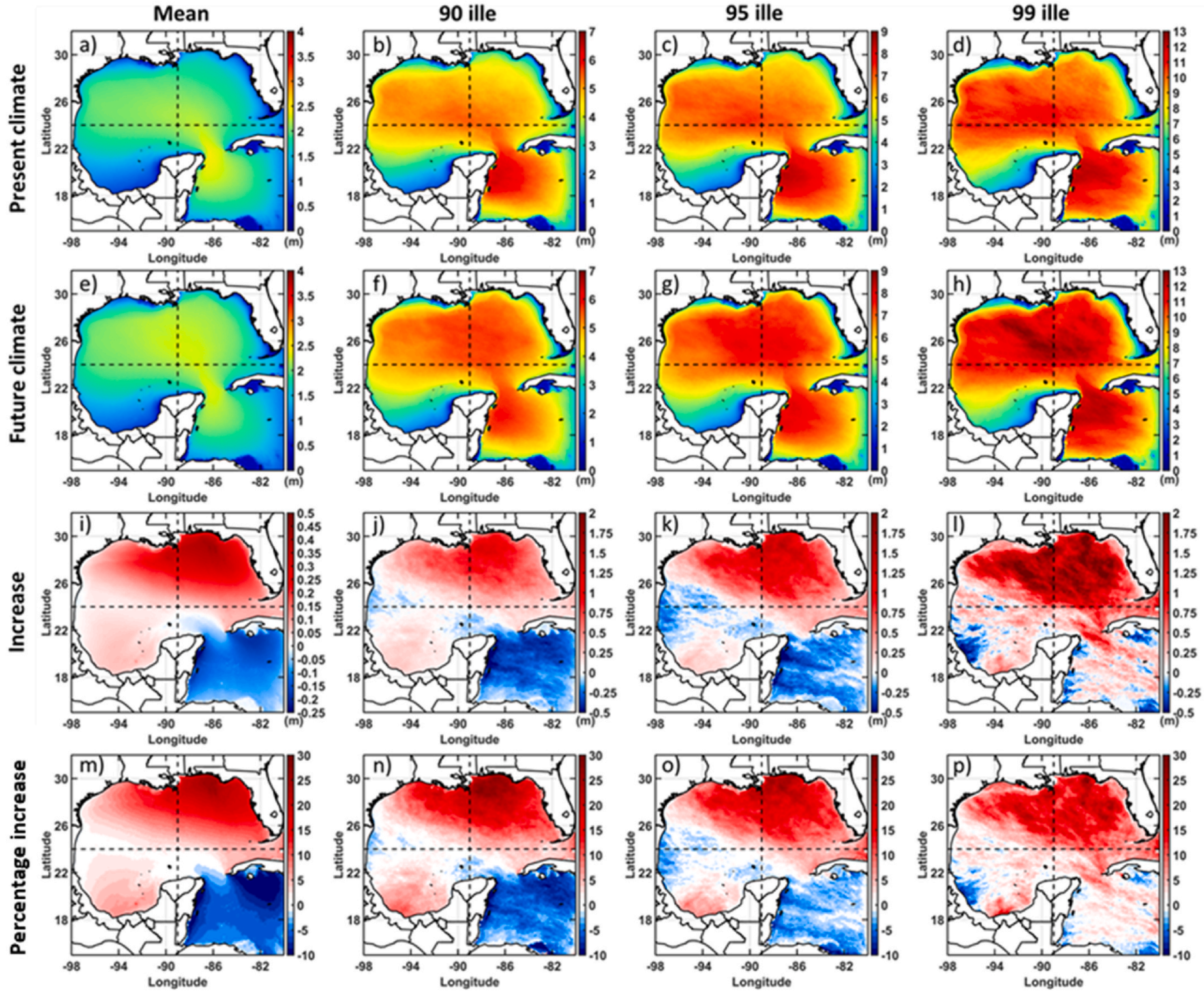

Fig. 9. Wave conditions for significant wave height for the present (a, b, c, d) and a future (e, f, g, h) wave climate model ensembles, as well as the change in significant wave height (i, j, k, l) and in percentage (m, n, o, p) in the future with respect to the present climate. The results show the mean (a, e, i, m), 90 %-ile (b, f, j, n), 95 %-ile (c, g, k, o) and 99 %-ile (d, h, l, p).

NE sector shows the largest increase among all percentiles and a generalized increase for the NW sector, except near the US-Mexico border. The SE sector shows generally a decrease in Hs in the future, although this decrease is much less than the increase in the NW sector and only for the mean and 90th and 95th-percentiles. For the 99th-percentile, there is a projected increase in Hs, which is smaller than that for the NE sector but similar to that for the NW sector near the US-Mexico border. The SW sector shows a smaller increase than the northern part of the GoM for the mean and 90th-percentiles of Hs. The SW sector for the 99th-percentile shows a clear increase in the southern part of the GoM, but a decrease towards the western part of the GoM, south of the US-Mexico border. Beyond the spatial shifts in Hs is the projected change of the underlying frequency of tropical-cyclone events (Table S1). Across the CMIP6 ensemble, there is ~5.4 % increase in total storms entering the GoM, driven by ~33 % rise in major hurricanes (Cat 3–5) and ~20 % decline in weaker systems (tropical storms and category 1 and 2 hurricanes). This redistribution with fewer low-intensity but more high-intensity storms is reflected in the future increases in extreme waves, particularly in the NE and NW sectors.

The results suggest that offshore oil extraction areas from Texas through Mississippi (where most oil and gas activities in the USA occur) could experience higher waves by the end of the century, as well as the Campeche Sound (where most oil and gas activities in Mexico occur) although with milder increases. For the offshore oil extraction area known as *Cinturón Plegado Perdido* south of the US-Mexico border, the results show a slight decrease in Hs, except for the most extreme waves (99th-percentile), where an increase similar to that of the Campeche Sound is observed. These results are consistent with the trends reported by (Ojeda et al., 2017) for the Mexican GoM.

3.3. Wave conditions based on return periods and implications on design

In the previous section, we divided the GoM into four sectors to describe our results; however, the API recommendations report Hs return periods within three regions specific to US GoM waters, as shown in Fig. 10 (West, Central, and East US) and defined in Section 2.5. Fig. 10 shows our calculated 15-, 25-, 50-, and 100-year return-period wave maps for the GoM ensemble under the present (Fig. 10a–d) and future (Fig. 10e–h) climates, the absolute changes (Fig. 10i–l) and the percentage changes (Fig. 10m–p). The figure also shows the boundaries of

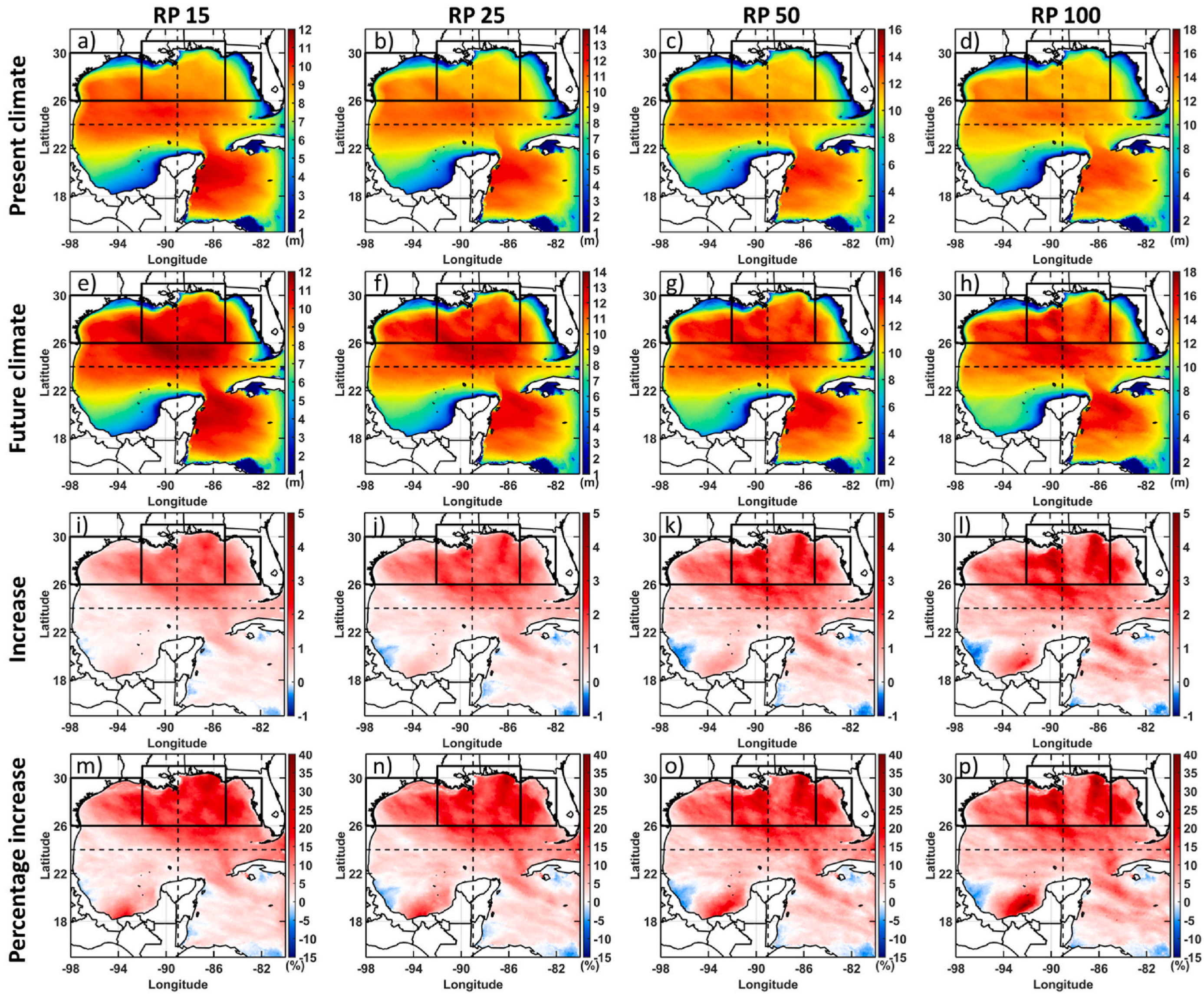

Fig. 10. Significant wave height for the 15, 25, 50, and 100-year return period (RP) obtained from the bias-corrected GCM-derived events ensemble for the present (a, b, c, d) and future (e, f, g, h) wave climates; increase in significant wave height (i, j, k, l) and in percentage (m, n, o, p) in the future with respect to the present climate. Solid black boxes represent areas defined by the API recommendations.

the regions (West, Central, and East US) as defined by (API, 2021) for presenting wave return periods. The ensembles were constructed using the waves resulting from the synthetic events derived from all GCMs. As can be seen from the different return periods, projections from most of the GCMs-based synthetic datasets show an increase in Hs return levels, except for a particular area in the SW sector. API regions will experience a significant increase in Hs, including the oil and gas exploitation areas offshore of Texas and Louisiana. These results are particularly relevant for assets whose metocean design basis is the 100-year return-period wave, for example, an L-1 platform (manned, non-evacuated, high--consequence of failure) in API RP 2MET (API, 2014). Our results show that this extreme increases markedly toward the end of the century. A prospect identified in 2025 would typically require ~10 years for appraisal, design, permitting, and construction, reaching first production around 2035. With a nominal 25 to 30-year design life (Wahab et al., 2020) that is often extended through life-extension programs (Stacey et al., 2008), the same installation could still be operating in 2070, precisely when our projections indicate a substantially higher 100-year Hs. The same timeline and exposure apply to other long-lived offshore assets, such as fixed-bottom offshore wind farms, that also rely on multi-decadal metocean criteria.

API (2007, 2014, 2021) has recommended using grid pooling (Heideman and Mitchell, 2009) to determine the wave conditions for various return periods within a specific area. This approach is particularly effective for tropical cyclones because of their low frequency, limited spatial extent, and inherent variability in storm tracks under various ambient conditions. In other words, different tropical cyclones will rarely pass by the same location more than once, which means that there is no hope for the statistics at a point to be reliable. However, certain regions share common oceanographic and atmospheric characteristics, so that extreme events can be considered equally likely to happen at any given point within that region. Therefore, extreme events are pooled together to create reliable statistics. Without grid pooling, a tropical cyclone that passes near an area may have followed a slightly different track, potentially leading to an underestimation of extreme wave conditions in that region. Although using an ensemble of TC waves derived from different GCMs helps address the randomness and limited population size of observed events, we implemented a simplified grid pooling analysis to derive Hs values for different return periods in the API-defined areas. Fig. 11 shows Hs results for different return periods

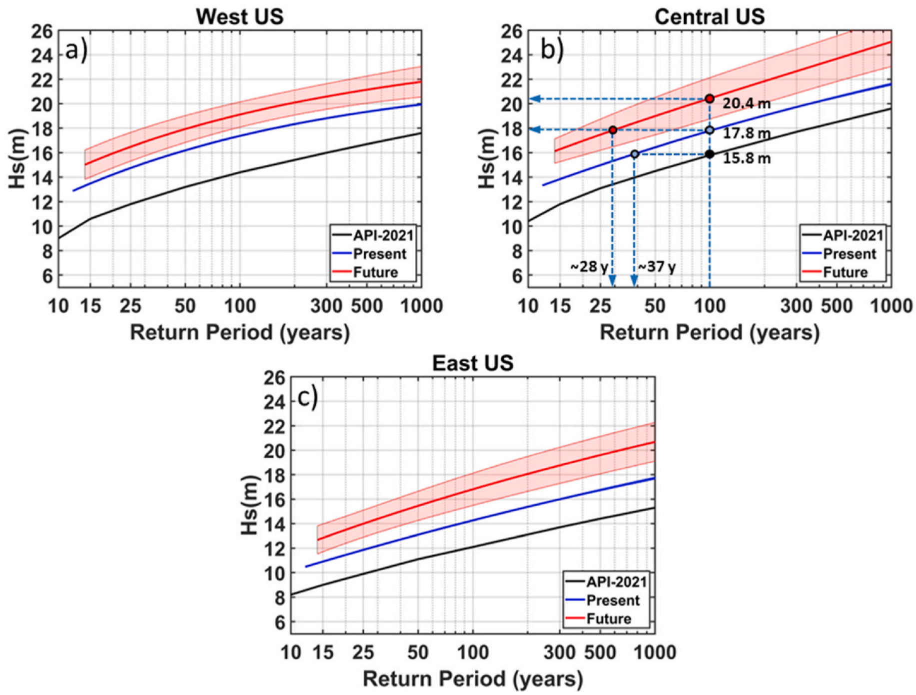

Fig. 11. Significant wave height return periods for the different API-defined areas in the northern Gulf of Mexico (denoted with the dash vertical lines in Fig. 2), a) West US, b) Central US, and c) East US, showing the return period curves for API, and the return periods obtained for the present and future climates as derived from the GCM events ensemble.

for both the present and future climates, as obtained using the peak over threshold method and applying the GPD. The results are compared to API (2021) recommended values, acknowledging API values as the industry standard.

The API values are smaller than our present-climate results using synthetic events, approximately by 2 m, which is consistent across different return periods, and being slightly higher in the West. For instance, in the Central area, the 100-year return period corresponds to a Hs of 17.8 m in our present-climate data while API recommends a value of 15.8 m, which in turn corresponds to a return period of approximately 37 years when considering the synthetic events in the present climate. The API underestimation stems from its reliance on historical event data, which may fail to capture rare high-intensity events, which as described in the introduction, has been the case several times in the past. Additionally, API's estimates are based on historical events since "*1900 to date*", while our study uses a historic frequency based on the reference climatology period 1980–2010. Synthetic events, despite inherent modeling uncertainties (e.g., parametric wind formulations and idealized storm structures), explicitly include plausible but rarely observed extremes and therefore may provide more representative estimates of high-intensity, low-probability events compared to short historical records alone. Although the synthetic approach might overestimate events due to the lack of feedback between the large-scale environment and downscaled events (Emanuel, 2021), our results are in agreement with past experience that using historical data alone may underestimate extreme waves. This is confirmed by the fact that the API has updated its guidelines following intense storm events or seasons with particularly high Accumulated Cyclone Energy (ACE). As such, our results using synthetic TCs underscore the limitations of relying solely on historical event-based estimates for wave climate characterization.

Unfortunately, we are unable to reproduce the API results for the period of 1980–2010, as the API (2014, 2021) standards lack a clear description of the methodological steps to determine the recommended Hs for different return periods. For example, API references proprietary hindcasts with vague and untraceable references (GUMSHOE and GOMOS), which are not publicly available, making independent verification impossible. Regarding grid pooling API refers to Heideman and Mitchell (2009), which states that there is "*no uniquely 'correct' way to do it*", adding uncertainty to how it is employed in determining the Hs recommendations for the different return periods in the three US areas. Additionally, the period considered for wave analysis remains ambiguous, as API states it includes data from "*1900 to the present*," without specifying an end date for the hindcast. This lack of transparency significantly limits reproducibility and reliability.

The hindcast period used in API introduces additional uncertainties, including whether extending the hindcast back to 1900 shifts the baseline to a different climate than the present-day conditions of the 21st century, whether historical storms provide sufficient data to correctly represent the low-probability tail, and whether storm events from the first half of the 20th century are even representative. In API (2007), it was acknowledged that pre-1950 storm data is unreliable due to limited observational capabilities before satellite and aircraft reconnaissance, and thus, it was not included in wave return period calculations. However, in API (2014, 2021), the methodology was expanded to include storm records dating back to 1900, despite known limitations in the intensity and frequency estimates for early hurricanes (Landsea, 2007). The inclusion of pre-satellite-era storms may introduce biases, artificially lowering return period wave height estimates due to systematic underreporting of extreme storms in earlier decades (as pointed out in API, 2007). Furthermore, the use of a historical baseline extending from 1900 to the present introduces additional biases besides the inaccuracies in storm intensity prior to 1950 (Landsea, 2007), due to the longer baseline diluting recent trends toward increased storm intensity (Kossin et al., 2020). A climatological baseline closer to the present day (such as 1980–2010) provides a more representative characterization of contemporary storm conditions. This issue is particularly critical as the present-day climatology of TCs is already changing (Kossin et al., 2020), meaning that past data may no longer be a reliable representation of the contemporary climate. However, this shorter, more recent period alone is insufficient for robust statistical estimation of low-probability extreme events, emphasizing the value of complementing observed data with synthetic events.

It is also important to note that the 100-year return period wave in API recommendations corresponds to a return period of less than 15 years in our synthetic TC results in a changing climate, denoting further the need to create robust statistics, while also addressing the effects of a non-stationary climate. If we only compare the results derived from synthetic TC, we find that the effect of climate change will lead to higher waves, with Hs approximately 2 m higher in the future. For instance, in the Central US area, the 100-year return period increases from 17.8 m in the present climate to 20.4 in the future climate, or said in other words, the 100-year return period waves would become a 28-year return period wave by the end of the century. To illustrate the implications on design, Fig. 12 shows the evolution of the 100-year return period design wave in the Central area, where the right axis corresponds to the grey line which is a linear interpolation of the return period change between 2010 and 2070, and each colored line shows the probability of occurrence (plotted on the left axis) of the design wave event over different structure service lives (5, 10, 20, 30, and 50 years), as derived from CIRIA-CUR-CETMEF (2007). In this plot, we can see that a structure designed based on the present 100-year return-period wave (17.8 m) has ~26 % probability of experiencing that event over a 30-year service life. By 2070, this probability is projected to increase to ~65 %. Such growth in exceedance likelihood shows that designs based on a stationary (present-day) wave climate could seriously underestimate the risk of structural failure in the future.

The results show the implications of using historical events, both for characterizing the present and future wave climates, and their implications in design. As such, we propose an alternative framework that integrates synthetic TCs to better capture the full range of potential storm intensities and their impact on wave conditions. This approach allows for a more robust representation of low-probability, high-impact wave events, which is crucial for offshore design under changing climate conditions, as we have demonstrated by comparing the values reported by the latest API recommendations (API, 2021) with those obtained using the peak over threshold method and applied the GPD to determine the return period Hs values. Integrating synthetic TCs into industry guidelines would provide more accurate values for the design of more resilient structures in a changing climate.

While this study quantifies future changes in the 100-year return-period Hs, the same non-stationary forcing also reshapes the full wave-energy spectrum that governs fatigue. Moderate sea states, roughly the 50th- to 95th-percentiles of Hs, usually account for the bulk of cumulative fatigue damage. Recent COWCLIP-based projections for

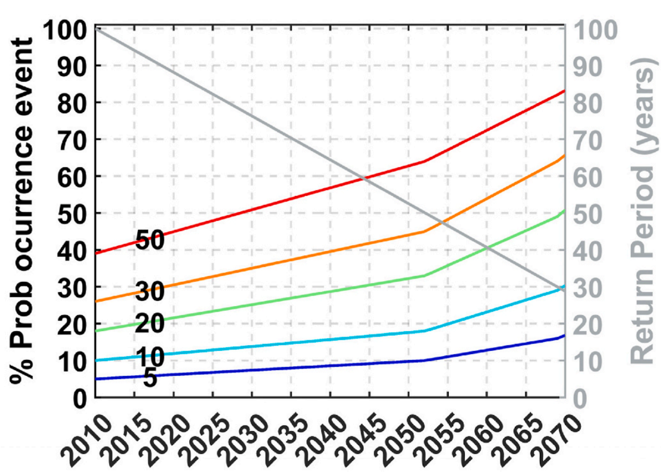

Fig. 12. Central US area percentage chance (left ordinate) of a 100-year return period wave in the present climate to occur as we transit into a future climate, where the colored lines indicate the projected design life of a structure, and the grey line shows the diminishing return period value (right ordinate) of the present climate 100-year return period wave as we approach a future climate.

the GoM (Appendini et al., 2025) indicate statistically significant increases across precisely this range. Merging such basin-scale, non--extreme wave statistics with the synthetic-storm catalogue employed here would yield a more complete picture of climate-driven fatigue loading. Future work should therefore integrate the two approaches to refine inspection intervals and remaining-life estimates, especially for components already operating close to their fatigue design factor.

A final consideration is that while our framework relies on fully spectral third-generation wave models to capture the detailed physics of TC-driven wave conditions, these models are computationally demanding and may be impractical for global-scale studies. In such cases, AI-based and parametric wave models such as those proposed by (Grossmann-Matheson et al., 2023, 2025), offer a more computationally efficient alternative. Nonetheless, we contend that fully spectral models should remain the benchmark for characterizing design wave parameters due to their superior ability to capture the underlying physics for wave modeling.

4. Conclusions

This study assessed the impact of climate change on extreme wave conditions in the Gulf of Mexico (GoM) using physics-based synthetic tropical cyclones (TCs) generated based on CMIP6 models. By using physics-based synthetic storm events and applying wave modeling and bias correction techniques, we addressed the limitations of historical data and general circulation models (GCMs), thereby providing a more robust characterization of present and future extreme wave climates. Our findings indicate that climate change will significantly alter the TC-driven wave conditions in the GoM —driven by a ~33 % increase in major hurricanes alongside a ~20 % decline in weaker storms. By the end of the 21st century, significant wave heights (Hs) are projected to increase by up to 30 %, with the most pronounced changes occurring in the northern region, particularly in the northeast sector of the GoM. While the southeastern sector may experience localized reductions in wave heights due to possible poleward shifts in TC activity, extreme wave events (99th-percentile) are still expected to increase across most domains. Equivalently, the increase in extreme wave heights implies that offshore structures will be considerably more likely to encounter one-in-a-hundred-years events within their lifetime.

These changes have critical implications for coastal and offshore infrastructure design. Relying on present stationary wave climate assumptions may lead to a significant underestimation of extreme wave hazards and an increased risk of structural failure. This underscores the necessity of adopting non-stationary wave climate approaches in engineering design, where return period assessments account for evolving climate conditions. A comparison with industry standards (API, 2021) highlights the limitations of traditional design methodologies that rely solely on historical data. API estimates for extreme waves tend to be lower than those derived from our synthetic TC wave events, reinforcing the concern that past observations alone may underestimate future risks.

Given the limitations of API's reliance on historical event-based estimates, our study proposes a proactive shift toward integrating synthetic TC-based wave modeling with GPD-based extreme value analysis as a more robust framework for wave climate assessment. This approach captures a broader range of extreme wave events, reduces dependence on short historical records, and ensures a more statistically sound basis for offshore structure design in a changing climate. Incorporating this methodology into industry standards would enhance predictive capabilities and reduce the need for reactive adjustments following severe hurricane seasons.

Future work should focus on refining probabilistic frameworks for extreme event characterization and exploring additional downscaling techniques to enhance the resolution and accuracy of TC-driven wave projections. For projecting wave climate in coastal waters, future studies can incorporate the effects of sea level rise to account for its impact on the water depth and, thus, the wave dynamics in shallow coastal waters.

CRediT authorship contribution statement

Christian M. Appendini: Writing – review & editing, Writing – original draft, Validation, Supervision, Resources, Project administration, Methodology, Investigation, Funding acquisition, Formal analysis, Conceptualization. **Pablo Ruiz-Salcines:** Writing – review & editing, Visualization, Validation, Software, Methodology, Investigation, Formal analysis, Data curation. **Rodrigo Duran:** Writing – review & editing, Resources, Methodology, Investigation. **Reza Marsooli:** Writing – review & editing, Resources, Methodology, Investigation. **ASM Alauddin Al Azad:** Writing – review & editing, Software, Methodology, Data curation. **Kerry Emanuel:** Writing – review & editing, Methodology, Investigation, Data curation.

Data availability

The data will be made available upon request. The original synthetic tropical cyclone datasets used in this study are freely available from Kerry Emanuel for research purposes. For the details and availability of the synthetic datasets, please refer to Emanuel (2021) (DOI: https://doi.org/10.1175/JCLI-D-20-0367.1).

Declaration of competing interest

The authors declare that they have no known competing financial interests or personal relationships that could have appeared to influence the work reported in this paper.

Acknowledgments

Centro Mexicano de Innovación en Energía del Océano, CEMIE-Océano (OLE-1), UNAM-DGAPA PAPIIT Project IA100418, and the U.S. Department of Energy's Office of Fossil Energy and Carbon Management, Upstream Research Division Office of Oil and Gas (through a support contract) provided funding for this study. CMA was supported by UNAM-DGAPA-PASPA and Aarhus University Research Foundation fellowships. PRS was partially supported by a Margarita Salas post-doctoral fellowship funded by the Spanish Ministry of Universities and the European Union through the NextGenerationEU programme. RM and AAA were supported by an Early-Career Research Fellowship from the Gulf Research Program of the National Academies of Sciences, Engineering, and Medicine. We thank DHI Inc. for providing the MIKE 21 SW license to perform this work. Simulations were done on the National Energy Technology Laboratory Joule Supercomputer. We would also like to thank Gonzalo Uriel Martín-Ruiz, José López-Gonzalez, Camilo Valdéz-Rendon, and Juan Alberto Gómez-Liera for their technical assistance with this work. We also acknowledge Rafael Meza-Padilla and Ana Ramirez-Manguilar for their contributions during the early stages of this study. The authors have no real or perceived financial conflicts of interest to declare. Neither the United States Government nor any agency thereof, nor any of its employees, nor the support contractor, nor any of their employees, makes any warranty, express or implied, or assumes any legal liability or responsibility for the accuracy, completeness, or usefulness of any information, apparatus, product, or process disclosed, or represents that its use would not infringe privately owned rights. Reference herein to any specific commercial product, process, or service by trade name, trademark, manufacturer, or otherwise does not necessarily constitute or imply its endorsement, recommendation, or favoring by the United States Government or any agency thereof. The views and opinions of authors expressed herein do not necessarily state or reflect those of the United States Government or any agency thereof. The content is solely the responsibility of the authors and does not necessarily represent the official views of the Gulf Research Program of the National Academies of Sciences, Engineering, and Medicine.

Appendix A. Supplementary data

Supplementary data to this article can be found online at https://doi.org/10.1016/j.oceaneng.2025.121685.

References

Alizadeh, M.J., Kavianpour, M.R., Kamranzad, B., Etemad-Shahidi, A., 2020. A distributed wind downscaling technique for wave climate modeling under future scenarios. Ocean Model. 145, 101513. https://doi.org/10.1016/j.ocemod.2019.101513.

Amante, C., Eakins, B.W., 2009. ETOPO1 1 Arc-Minute Global Relief Model: Procedures, Data Sources and Analysis.

API, 2007. Interim guidance on hurricane conditions in the Gulf of Mexico. API Recommended Practice, 2INT-MET 54.

API, 2014. Derivation of metocean design and operating conditions. ANSI/API Recommended Practice 2MET. *API Recommended Practice*, 2MET (first ed.), p. 178.

API, 2021. Derivation of metocean design and operating conditions. ANSI/API Recommended Practice 2MET. *API Recommended Practice*, 2MET (second ed.), p. 265.

Appendini, C.M., Pedrozo-Acuña, A., Meza-Padilla, R., Torres-Freyermuth, A., Cerezo-Mota, R., López-González, J., Ruiz-Salcines, P., 2017. On the role of climate change on wind waves generated by tropical cyclones in the Gulf of Mexico. Coast. Eng. J. 59 (2). https://doi.org/10.1142/S0578563417400010.

Appendini, C.M., Ruiz-Salcines, P., Marsooli, R., Cerezo-Mota, R., 2025. Assessing the effects of climate change on the Gulf of Mexico wave climate using the COWCLIP framework and the PRECIS regional climate model. Ocean Model. 194. https://doi.org/10.1016/j.ocemod.2024.102486.

Appendini, C.M., Torres-Freyermuth, A., Salles, P., López-González, J., Mendoza, E.T., 2014. Wave climate and trends for the Gulf of Mexico: a 30-yr wave hindcast. J. Clim. 27 (4), 1619–1632. https://doi.org/10.1175/JCLI-D-13-00206.1.

Austin, D.E., Priest, T., Penney, L., Pratt, J., Pulsipher, A.G., Abel, J., Taylor, J., 2008. History of the offshore oil and gas industry in southern Louisiana, Volume I.

Baghanian, S., Alizadeh, M.J., 2022. Wave climate projection in the Persian gulf: an ensemble of statistically downscaled CMIP6-GCMs. Ocean Eng. 266, 112821. https://doi.org/10.1016/j.oceaneng.2022.112821.

Baker, A.J., Vannière, B., Vidale, P.L., 2024. On the realism of tropical cyclone intensification in global storm-resolving climate models. Geophys. Res. Lett. 51 (17). https://doi.org/10.1029/2024GL109841.

Battjes, J.A.A., Janssen, J.P.F.M., 1978. Energy loss and set-up due to breaking of random waves. Proceedings of the 16th International Conference on Coastal Engineering 1 (16), 569–587. https://doi.org/10.9753/icce.v16.

Bloemendaal, N., de Moel, H., Martinez, A.B., Muis, S., Haigh, I.D., van der Wiel, K., Haarsma, R.J., Ward, P.J., Roberts, M.J., Dullaart, J.C.M., Aerts, J.C.J.H., 2022. A globally consistent local-scale assessment of future tropical cyclone risk. Sci. Adv. 8 (17), eabm8438. https://doi.org/10.1126/sciadv.abm8438.

Caires, S., 2016. A comparative simulation study of the annual maxima and the peaks-over-threshold methods. J. Offshore Mech. Arc. Eng. 138 (5). https://doi.org/10.1115/1.4033563.

Camargo, S.J., 2013. Global and regional aspects of tropical cyclone activity in the CMIP5 models. J. Clim. 26 (24), 9880–9902. https://doi.org/10.1175/JCLI-D-12-00549.1.

Camargo, S.J., Murakami, H., Bloemendaal, N., Chand, S.S., Deshpande, M.S., Dominguez-Sarmiento, C., González-Alemán, J.J., Knutson, T.R., Lin, I.I., Moon, I.J., Patricola, C.M., Reed, K.A., Roberts, M.J., Scoccimarro, E., Tam, Francis, C.Y., Wallace, E.J., Wu, L., Yamada, Y., Zhang, W., Zhao, H., 2023. An update on the influence of natural climate variability and anthropogenic climate change on tropical cyclones. Trop. Cycl. Res. Rev. 12 (3), 216–239. https://doi.org/10.1016/j.tcrr.2023.10.001.

CIRIA-CUR-CETMEF, 2007. *The Rock Manual. the Use of Rock in Hydraulic Engineering* (2Nd Editio). CIRIA, London, C683. https://www.kennisbank-waterbouw.nl/DesignCodes/rockmanual/.

Coles, S., 2001. An Introduction to Statistical Modeling of Extreme Values. Springer, UK.

Cruz, A.M., Krausmann, E., 2008. Damage to offshore oil and gas facilities following hurricanes katrina and rita: an overview. J. Loss Prev. Process. Ind. 21 (6), 620–626. https://doi.org/10.1016/j.jlp.2008.04.008.

Danabasoglu, G., Lamarque, J.-F., Bacmeister, J., Bailey, D.A., DuVivier, A.K., Edwards, J., Emmons, L.K., Fasullo, J., Garcia, R., Gettelman, A., Hannay, C., Holland, M.M., Large, W.G., Lauritzen, P.H., Lawrence, D.M., Lenaerts, J.T.M., Lindsay, K., Lipscomb, W.H., Mills, M.J., et al., 2020. The community Earth system model version 2 (CESM2). J. Adv. Model. Earth Syst. 12 (2). https://doi.org/10.1029/2019MS001916.

Demuth, J.L., DeMaria, M., Knaff, J.A., 2006. Improvement of advanced microwave sounding unit tropical cyclone intensity and size estimation algorithms. J. Appl. Meteorol. Climatol. 45 (11), 1573–1581. https://doi.org/10.1175/JAM2429.

Déqué, M., 2007. Frequency of precipitation and temperature extremes over France in an anthropogenic scenario: model results and statistical correction according to observed values. Global Planet. Change 57 (1–2), 16–26. https://doi.org/10.1016/j.gloplacha.2006.11.030.

Dunn, F.P., 1994. Deepwater production: 1950-2000. Proceedings of the Annual Offshore Technology Conference, pp. 921–928. https://doi.org/10.4043/7627-MS.

Dunne, J.P., Horowitz, L.W., Adcroft, A.J., Ginoux, P., Held, I.M., John, J.G., Krasting, J. P., Malyshev, S., Naik, V., Paulot, F., Shevliakova, E., Stock, C.A., Zadeh, N., Balaji, V., Blanton, C., Dunne, K.A., Dupuis, C., Durachta, J., Dussin, R., et al., 2020.

The GFDL Earth system model version 4.1 (GFDL-ESM 4.1): overall coupled model description and simulation characteristics. J. Adv. Model. Earth Syst. 12 (11). https://doi.org/10.1029/2019MS002015.

Eldeberky, Y., Battjes, J.A., 1995. Parameterization of triad interactions in wave energy models. In: Dally, W.R., Zeidler, R.B. (Eds.), Coastal Dynamics '95, pp. 140–148.

Eldeberky, Y., Battjes, J.A., 1996. Spectral modeling of wave breaking: application to boussinesq equations. J. Geophys. Res. 101 (C1), 1253. https://doi.org/10.1029/95JC03219.

Emanuel, K., 2004. Tropical cyclone energetics and structure. In: Fedorovich, E., Rotunno, R., Stevens, B. (Eds.), *Atmospheric Turbulence and Mesoscale Meteorology* (Issue 1944. Cambridge University Press, p. 280. https://doi.org/10.1017/cbo9780511735035.010.

Emanuel, K., 2010. Tropical cyclone activity downscaled from NOAA-CIRES reanalysis, 1908–1958. J. Adv. Model. Earth Syst. 2. https://doi.org/10.3894/james.2010.2.1.

Emanuel, K., 2013. Downscaling CMIP5 climate models shows increased tropical cyclone activity over the 21st century. Proc. Natl. Acad. Sci. U.S.A. 110 (30), 12219–12224. https://doi.org/10.1073/pnas.1301293110.

Emanuel, K., 2021. Response of global tropical cyclone activity to increasing CO2: results from downscaling CMIP6 models. J. Clim. 34 (1), 57–70. https://doi.org/10.1175/JCLI-D-20-0367.1.

Emanuel, K.A., 2013. Downscaling CMIP5 climate models shows increased tropical cyclone activity over the 21st century. Proc. Natl. Acad. Sci. U.S.A. 110 (30), 12219–12224. https://doi.org/10.1073/pnas.1301293110.

Emanuel, K., Ravela, S., Vivant, E., Risi, C., 2006. A statistical deterministic approach to hurricane risk assessment. Bull. Am. Meteorol. Soc. 87 (3), 299–314. https://doi.org/10.1175/BAMS-87-3-299.

Emanuel, K., Sundararajan, R., Williams, J., Manuel, K., Sundararajan, R., Williams, J., Emanuel, K., Sundararajan, R., Williams, J., 2008. Hurricanes and global warming: results from downscaling IPCC AR4 simulations. Bull. Am. Meteorol. Soc. 89 (3), 347–367. https://doi.org/10.1175/BAMS-89-3-347.

Grossmann-Matheson, G., Young, I.R., Alves, J.H., Meucci, A., 2023. Development and validation of a parametric tropical cyclone wave height prediction model. Ocean Eng. 283. https://doi.org/10.1016/j.oceaneng.2023.115353.

Grossmann-Matheson, G., Young, I.R., Meucci, A., Alves, J.H., 2024a. Global changes in extreme tropical cyclone wave heights under projected future climate conditions. Sci. Rep. 14 (1). https://doi.org/10.1038/s41598-024-82892-9.

Grossmann-Matheson, G., Young, I.R., Meucci, A., Alves, J.H., 2024b. Global tropical cyclone extreme wave height climatology. Sci. Rep. 14 (1). https://doi.org/10.1038/s41598-024-54691-9.

Grossmann-Matheson, G., Young, I.R., Meucci, A., Alves, J.H., Tamizi, A., 2025. A model for the spatial distribution of ocean wave parameters in tropical cyclones. Ocean Eng. 317. https://doi.org/10.1016/j.oceaneng.2024.120091.

Hasselmann, S., Hasselmann, K., 1985. Computations and parameterizations of the nonlinear energy transfer in a gravity-wave spectrum. Part I: a new method for efficient computations of the exact nonlinear transfer integral. J. Phys. Oceanogr. 15 (11, Nov. 1985), 1369–1377. https://doi.org/10.1175/1520-0485(1985)015<1369:capotn>2.0.co.

Hasselmann, S., Hasselmann, K., Allender, J.H., Barnett, T.P., 1985. Computations and parameterizations of the nonlinear energy transfer in a gravity-wave spectrum. Part II: parameterizations of the nonlinear energy transfer for application in wave models. J. Phys. Oceanogr. 15, 1378–1391 file:///C:/Users/CAppendiniA/CMA/03 Apoyo/Biblioteca/Mendeley/Hasselmann et al. - 1985 - Computations and parameterizations of the nonlinear energy transfer in a gravity-wave spectrum. Part II Param.pdf.

Heideman, J.C., Mitchell, D.A., 2009. Grid point pooling in extreme value analysis of hurricane hindcast data. J. Waterw. Port, Coast. Ocean Eng. 135 (2), 31–37. https://doi.org/10.1061/(ASCE)0733-950X(2009)135:2(31.

Hemer, M.A., Wang, X.L., Weisse, R., Swail, V.R., 2012. Advancing wind-waves climate science: the COWCLIP project. Bull. Am. Meteorol. Soc. 93 (6), 791–796. https://doi.org/10.1175/BAMS-D-11-00184.1.

Hill, K.A., Lackmann, G.M., 2011. The impact of future climate change on TC intensity and structure: a downscaling approach. J. Clim. 24 (17), 4644–4661. https://doi.org/10.1175/2011JCLI3761.1.

Holland, G.J., Belanger, J.I., Fritz, A., 2010. A revised model for radial profiles of hurricane winds. Mon. Weather Rev. 138 (12), 4393–4401. https://doi.org/10.1175/2010MWR3317.1.

Horowitz, A., 2020. *Katrina: a History, 1915–2015* (First). Harvard University Press.

Jamous, M., Marsooli, R., Miller, J.K., 2023. Physics-based modeling of climate change impact on hurricane-induced coastal erosion hazards. Npj Climate and Atmospheric Science 6 (1), 86. https://doi.org/10.1038/s41612-023-00416-0.

Janssen, P.A.E.M., 1989. Wave-induced stress and the drag of air flow over sea waves. J. Phys. Oceanogr. 19, 745–754.

Janssen, P.A.E.M., 1991. Quasi-linear theory of wind wave generation applied to wave forecasting. J. Phys. Oceanogr. 21, 1631–1642. http://journals.ametsoc.org/doi/pdf/10.1175/1520-0485(1991)021%3C1631:QLTOWW%3E2.0.CO.

Janssen, P.A.E.M., Lionello, P., Zambresky, L., 1989. On the interaction of wind and waves. Phil. Trans. Roy. Soc. Lond. Math. Phys. Sci. 329 (1604), 289–301. https://doi.org/10.1098/rsta.1989.0077.

Johnson, H.K., Kofoed-Hansen, H., 2000. Influence of bottom friction on sea surface roughness and its impact on shallow water wind wave modeling. J. Phys. Oceanogr. 30 (7), 1743–1756.

Judt, F., Klocke, D., Rios-Berrios, R., Vanniere, B., Ziemen, F., Auger, L., Biercamp, J., Bretherton, C., Chen, X., Düben, P., Hohenegger, C., Khairoutdinov, M., Kodama, C., Kornblueh, L., Lin, S.-J., Nakano, M., Neumann, P., Putman, W., Röber, N., et al., 2021. Tropical cyclones in global storm-resolving models. Journal of the Meteorological Society of Japan. Ser. 99 (3), 2021–2029. https://doi.org/10.2151/jmsj.2021-029.

Kaiser, M.J., Yu, Y., 2010. The impact of hurricanes gustav and ike on offshore oil and gas production in the Gulf of Mexico. Appl. Energy 87 (1), 284–297. https://doi.org/10.1016/j.apenergy.2009.07.014.

Knapp, K.R., Kruk, M.C., Levinson, D.H., Diamond, H.J., Neumann, C.J., 2010. The international best track archive for climate stewardship (IBTrACS). Bull. Am. Meteorol. Soc. 91 (3), 363–376. https://doi.org/10.1175/2009BAMS2755.1.

Knutson, T., Camargo, S.J., Chan, J.C.L., Emanuel, K., Ho, C.-H., Kossin, J., Mohapatra, M., Satoh, M., Sugi, M., Walsh, K., Wu, L., 2020. Tropical cyclones and climate change assessment: part II: projected response to anthropogenic warming. Bull. Am. Meteorol. Soc. 101 (3), E303–E322. https://doi.org/10.1175/BAMS-D-18-0194.1.

Komen, G.J., Cavaleri, L., Donelan, M., Hasselmann, K., Hasselmann, S., Janssen, P.A.E.M., 1994. Dynamics and Modelling of Ocean Waves. Cambridge University Press file:///C:/Users/CAppendiniA/CMA/03 Apoyo/Biblioteca/Mendeley/Komen et al. - 1994 - Dynamics and modelling of ocean waves.pdf.

Kossin, J.P., Emanuel, K.A., Vecchi, G.A., 2014. The poleward migration of the location of tropical cyclone maximum intensity. Nature 509 (7500), 349–352. https://doi.org/10.1038/nature13278.

Kossin, J.P., Knapp, K.R., Olander, T.L., Velden, C.S., 2020. Global increase in major tropical cyclone exceedance probability over the past four decades. Proc. Natl. Acad. Sci. 117 (22), 11975–11980. https://doi.org/10.1073/pnas.1920849117.

Landsea, C.W., 2007. Counting Atlantic tropical cyclones back to 1900. Eos (Wroc.) 88 (18), 197–208. https://doi.org/10.1029/2007EO180001.

Leijnse, T.W.B., Giardino, A., Nederhoff, K., Caires, S., 2022. Generating reliable estimates of tropical-cyclone-induced coastal hazards along the Bay of Bengal for current and future climates using synthetic tracks. Nat. Hazards Earth Syst. Sci. 22 (6), 1863–1891. https://doi.org/10.5194/nhess-22-1863-2022.

Li, H., Sheffield, J., Wood, E.F., 2010. Bias correction of monthly precipitation and temperature fields from intergovernmental panel on climate change AR4 models using equidistant quantile matching. J. Geophys. Res. Atmos. 115 (10). https://doi.org/10.1029/2009JD012882.

Lobeto, H., Menendez, M., Losada, I.J., 2021. Future behavior of wind wave extremes due to climate change. Sci. Rep. 11 (1). https://doi.org/10.1038/s41598-021-86524-4.

Mangiavacchi, A., Rodenbusch, G., Radford, A., Wisch, D., 2005. API offshore structure standards: RP 2A and much more. Offshore Technology Conference 2195–2200. https://doi.org/10.4043/17697-MS, 2005-May.

Marks, D.G., 1992. The Beta and Advection Model for Hurricane Track Forecasting.

Marsooli, R., Jamous, M., Miller, J.K., 2021. Climate change impacts on wind waves generated by major tropical cyclones off the Coast of New Jersey, USA. Frontiers in Built Environment 7. https://doi.org/10.3389/fbuil.2021.774084.

Martínez-Asensio, A., Marcos, M., Jordà, G., Gomis, D., 2013. Calibration of a new wind-wave hindcast in the Western mediterranean. J. Mar. Syst. 121–122, 1–10. https://doi.org/10.1016/j.jmarsys.2013.04.006.

Méndez, F.J., Menéndez, M., Luceño, A., Losada, I.J., 2006. Estimation of the long-term variability of extreme significant wave height using a time-dependent peak over threshold (POT) model. J. Geophys. Res.: Oceans 111 (7). https://doi.org/10.1029/2005JC003344.

Meza-Padilla, R., Appendini, C.M.C.M., Pedrozo-Acuña, A., 2015. Hurricane-induced waves and storm surge modeling for the Mexican Coast. Ocean Dyn. 65 (8), 1199–1211. https://doi.org/10.1007/s10236-015-0861-7.

Mori, N., Yasuda, T., Mase, H., Tom, T., Oku, Y., 2010. Projection of extreme wave climate change under global warming. Hydrological Research Letters 4, 15–19. https://doi.org/10.3178/HRL.4.15.

Morim, J., Hemer, M., Wang, X.L., Cartwright, N., Trenham, C., Semedo, A., Young, I., Bricheno, L., Camus, P., Casas-Prat, M., Erikson, L., Mentaschi, L., Mori, N., Shimura, T., Timmermans, B., Aarnes, O., Breivik, Ø., Behrens, A., Dobrynin, M., et al., 2019. Robustness and uncertainties in global multivariate wind-wave climate projections. Nat. Clim. Change 9 (9), 711–718. https://doi.org/10.1038/s41558-019-0542-5.

Morim, J., Wahl, T., Vitousek, S., Santamaria-Aguilar, S., Young, I., Hemer, M., 2023. Understanding uncertainties in contemporary and future extreme wave events for broad-scale impact and adaptation planning. https://www.science.org.

Müller, W.A., Jungclaus, J.H., Mauritsen, T., Baehr, J., Bittner, M., Budich, R., Bunzel, F., Esch, M., Ghosh, R., Haak, H., Ilyina, T., Kleine, T., Kornblueh, L., Li, H., Modali, K., Notz, D., Pohlmann, H., Roeckner, E., Stemmler, I., et al., 2018. A higher-resolution version of the max planck institute Earth system model (MPI-ESM1.2-HR). J. Adv. Model. Earth Syst. 10 (7), 1383–1413. https://doi.org/10.1029/2017MS001217.

NOAA National Centers for Environmental Information, 2023. Coastal Relief Models (Crms), vol. 3. NOAA National Centers for Environmental Information. https://doi.org/10.25921/5ZN5-KN44.

Ojeda, E., Appendini, C.M., Mendoza, E.T., 2017. Storm-wave trends in Mexican waters of the Gulf of Mexico and Caribbean Sea. Nat. Hazards Earth Syst. Sci. 17 (8). https://doi.org/10.5194/nhess-17-1305-2017.

Panchang, V., Jeong, C.K., Demirbilek, Z., 2013. Analyses of extreme wave heights in the Gulf of Mexico for offshore engineering applications. J. Offshore Mech. Arctic Eng. 135 (3), 31104–31115. https://doi.org/10.1115/1.4023205.

Parker, K., Hill, D.F., 2017. Evaluation of bias correction methods for wave modeling output. Ocean Model. 110, 52–65. https://doi.org/10.1016/j.ocemod.2016.12.008.

Pérez-Alarcón, A., Fernández-Alvarez, J.C., Coll-Hidalgo, P., 2023. Global increase of the intensity of tropical cyclones under global warming based on their maximum potential intensity and CMIP6 models. Environmental Processes 10 (2). https://doi.org/10.1007/s40710-023-00649-4.

Powell, M.D., Houston, S.H., 1996. Hurricane andrew's landfall in south Florida. Part II: surface wind fields and potential real-time applications. Weather Forecast. 11 (3), 329–349. https://doi.org/10.1175/1520-0434(1996)011<0329:HALISF>2.0.CO.

Powell, M.D., Houston, S.H., Reinhold, T.A., 1996. Hurricane andrew's landfall in south Florida. Part I: standardizing measurements for documentation of surface wind fields. Weather Forecast. 11 (3), 304–328. https://doi.org/10.1175/1520-0434(1996)011<0304:HALISF>2.0.CO.

Powell, M.D., Murillo, S., Dodge, P., Uhlhorn, E., Gamache, J., Cardone, V., Cox, A., Otero, S., Carrasco, N., Annane, B., Fleur, R. St, 2010. Reconstruction of hurricane Katrina's wind fields for storm surge and wave hindcasting. Ocean Eng. 37 (1), 26–36. https://doi.org/10.1016/j.oceaneng.2009.08.014.

Roberts, M.J., Camp, J., Seddon, J., Vidale, P.L., Hodges, K., Vannière, B., Mecking, J., Haarsma, R., Bellucci, A., Scoccimarro, E., Caron, L., Chauvin, F., Terray, L., Valcke, S., Moine, M., Putrasahan, D., Roberts, C.D., Senan, R., Zarzycki, C., et al., 2020a. Projected future changes in tropical cyclones using the CMIP6 HighResMIP multimodel ensemble. Geophys. Res. Lett. 47 (14). https://doi.org/10.1029/2020GL088662.

Roberts, M.J., Camp, J., Seddon, J., Vidale, P.L., Hodges, K., Vanniere, B., Mecking, J., Haarsma, R., Bellucci, A., Scoccimarro, E., Caron, L.-P., Chauvin, F., Terray, L., Valcke, S., Moine, M.-P., Putrasahan, D., Roberts, C., Senan, R., Zarzycki, C., Ullrich, P., 2020b. Impact of model resolution on tropical cyclone simulation using the HighResMIP–PRIMAVERA multimodel ensemble. J. Clim. 33 (7), 2557–2583. https://doi.org/10.1175/JCLI-D-19-0639.1.

Rohith, A.N., Cibin, R., 2024. An extremes-weighted empirical quantile mapping for global climate model data bias correction for improved emphasis on extremes. Theor. Appl. Climatol. 155 (6), 5515–5523. https://doi.org/10.1007/s00704-024-04965-z.

Sellar, A.A., Walton, J., Jones, C.G., Wood, R., Abraham, N.L., Andrejczuk, M., Andrews, M.B., Andrews, T., Archibald, A.T., de Mora, L., Dyson, H., Elkington, M., Ellis, R., Florek, P., Good, P., Gohar, L., Haddad, S., Hardiman, S.C., Hogan, E., et al., 2020. Implementation of U.K. Earth system models for CMIP6. J. Adv. Model. Earth Syst. 12 (4). https://doi.org/10.1029/2019MS001946.

Shi, J., Feng, X., Toumi, R., Zhang, C., Hodges, K.I., Tao, A., Zhang, W., Zheng, J., 2024. Global increase in tropical cyclone ocean surface waves. Nat. Commun. 15 (1). https://doi.org/10.1038/s41467-023-43532-4.

Sørensen, O.R., Kofoed-Hansen, H., Rugbjerg, M., Sørensen, L.S., 2004. A third-generation spectral wave model using an unstructured finite volume technique. Proceedings of the 29th International Conference on Coastal Engineering, 2005-Janua, pp. 894–906. https://doi.org/10.1142/9789812701916-0071.

Stacey, A., Birkinshaw, M., Sharp, J.V., 2008. Life extension issues for ageing offshore installations. Materials Technology; CFD and VIV 5, 199–215. https://doi.org/10.1115/OMAE2008-57411.

Studholme, J., Fedorov, A.V., Gulev, S.K., Emanuel, K., Hodges, K., 2022. Poleward expansion of tropical cyclone latitudes in warming climates. Nat. Geosci. 15 (1), 14–28. https://doi.org/10.1038/s41561-021-00859-1. Nature Research.

Tamizi, A., Young, I.R., 2024. A dataset of global tropical cyclone wind and surface wave measurements from buoy and satellite platforms. Sci. Data 11 (1), 106. https://doi.org/10.1038/s41597-024-02955-4.

Tatebe, H., Ogura, T., Nitta, T., Komuro, Y., Ogochi, K., Takemura, T., Sudo, K., Sekiguchi, M., Abe, M., Saito, F., Chikira, M., Watanabe, S., Mori, M., Hirota, N., Kawatani, Y., Mochizuki, T., Yoshimura, K., Takata, K., O'ishi, R., et al., 2019. Description and basic evaluation of simulated mean state, internal variability, and climate sensitivity in MIROC6. Geosci. Model Dev. (GMD) 12 (7), 2727–2765. https://doi.org/10.5194/gmd-12-2727-2019.

Timmermans, B., Stone, D., Wehner, M., Krishnan, H., 2017. Impact of tropical cyclones on modeled extreme wind-wave climate. Geophys. Res. Lett. 44 (3), 1393–1401. https://doi.org/10.1002/2016GL071681.

Tolman, H.L., 2002. Alleviating the garden sprinkler effect in wind wave models. Ocean Model. 4, 269–289.

Wahab, M.M.A., Kurian, V.J., Liew, M.S., Kim, D.K., 2020. Condition assessment techniques for aged fixed-type offshore platforms considering decommissioning: a historical review. J. Mar. Sci. Appl. 19 (4), 584–614. https://doi.org/10.1007/s11804-020-00181-z.

Wang, X.L., Feng, Y., Swail, V.R., 2015. Climate change signal and uncertainty in CMIP5-based projections of global ocean surface wave heights. J. Geophys. Res.: Oceans 120 (5), 3859–3871. https://doi.org/10.1002/2015JC010699.

Wisch, D.J., Puskar, F.J., Laurendine, T.T., O'Connor, P.E., Versowsky, P.E., Bucknell, J., 2004. An update on API RP 2A section 17 for the assessment of existing platforms. Offshore Technology Conference (3), 2079–2089. https://doi.org/10.4043/16820-MS.